

博士論文

論文題目 Neocortical Rebound Depolarization and its Impact on
Visual Processing

(視覚皮質における遅延性応答の発生源および視覚機能の調節)

氏名 舟山 健太

CONTENTS

Chapter 1 Impact of Neocortical Rebound Depolarization on Visual Processing

Abstract · · · · ·	4
Introduction · · · · ·	5
Materials and Methods · · · · ·	7
Results · · · · ·	18
Discussion · · · · ·	28
Figures · · · · ·	33

Chapter 2 Origin of Neocortical Rebound Depolarization

Abstract · · · · ·	58
Introduction · · · · ·	59
Materials and Methods · · · · ·	60
Results · · · · ·	64
Discussion · · · · ·	70
Figures · · · · ·	73
References · · · · ·	84
Acknowledgements · · · · ·	95

Chapter 1

Impact of Neocortical Rebound Depolarization on Visual Processing

ABSTRACT

Animals are constantly exposed to the time-varying visual world. Because visual perception is modulated by immediately prior visual experience, visual cortical neurons may register recent visual history into a specific form of offline activity and link it to later visual input. To examine how preceding visual inputs interact with upcoming information at the single neuron level, we designed a simple stimulation protocol in which a brief, orientated flashing stimulus was subsequently coupled to visual stimuli with identical or different features. Using *in vivo* whole-cell patch-clamp recording and functional two-photon calcium imaging from the primary visual cortex (V1) of awake mice, we discovered that a flash of sinusoidal grating *per se* induces an early, transient activation as well as a long-delayed reactivation in V1 neurons. This late response, which started hundreds of milliseconds after the flash and persisted for approximately 2 s, was also observed in human V1 electroencephalogram. When another drifting grating stimulus arrived during the late response, the V1 neurons exhibited a sublinear, but apparently increased response especially to the same grating orientation. In behavioral tests of mice and humans, the flashing stimulation enhanced the detection power of the identically orientated visual stimulation only when the second stimulation was presented during the time window of the late response. Therefore, V1 late responses likely provide a neural basis for admixing temporally separated stimuli and extracting identical features in time-varying visual environments.

INTRODUCTION

The primary visual cortex (V1) has been used as an experimental model to study cortical responses to sensory input. V1 receives direct synaptic inputs from the dorsal lateral geniculate nucleus (dLGN) of the thalamus and provides the output of its computation to higher-order cortical areas [1,2]. This route, commonly known as the feed forward pathway, contributes to the hierarchical neural processing of specific visual features, such as orientation, direction, color, and motion. Classical visual processing models consider V1 as a passive relay station for visual information; that is, V1 encodes instantaneous information by transiently responding to the present stimulus feature. However, recent evidence has demonstrated that V1 activity persists over time [3-7] and even propagates throughout the V1 network [8,9]. This complex activity is likely associated with the representation of reward timing [4,5], iconic memory [10,11], and working memory [12-14]. Indeed, reverberatory neuronal activity within neocortical circuitry has been proposed as a potential mechanism for short-term storage of information [15,16].

How does V1 encode the external world while under a constant flow of visual stimuli? The measurement of cortical dynamics has revealed that V1 response tuning evolves with time [17], during which it may interfere with later V1 information [18]. Indeed, preceding visual stimuli are reported to modulate visual perception after brief stimulus-onset asynchrony (SOA) [19-22]. Therefore, post-stimulus V1 activity appears to intermingle with the subsequent visual information, which produces a complex output [23-25].

In this study, we discovered a novel V1 activation pattern in non-anesthetized mice; in virtually all V1 neurons, an oriented flashing light induced biphasic membrane

voltage (V_m) responses that consisted of an early, transient depolarization and a late, slow depolarization. The late response exhibited high orientation selectivity, which indicates that V1 maintains the information of a recent stimulus with high fidelity for some time. Flash-induced late response was also observed using electroencephalogram (EEG) recordings in humans, suggesting that a long-delayed V1 reactivation prevails in mammals. To understand the effect of the late response on the upcoming visual input, we paired a flashing stimulus to another visual stimulus with a time lag. Flashes modulated the V1 response to the subsequent input in an orientation-selective manner. The flash-induced selective modulation was also replicated in the psychophysical parameters of mice and humans.

MATERIALS AND METHODS

Ethical approval

Animal experiments were performed with the approval of the animal experiment ethics committee at the University of Tokyo (approval number: 21-6) and according to the University of Tokyo's guidelines for the care and use of laboratory animals. In human studies, the experimental protocol was approved by the Human Research Ethics Committee of the University of Tokyo (approval number: 24-3) and the Center for Information and Neural Networks (approval number: 1312260010). All participants were provided oral and written informed consents, and they signed the consent forms prior to each experiment.

Animal preparation for recordings

Postnatal days (P) 28-35 male C57BL/6J mice (Japan SLC, Shizuoka, Japan) were used in the animal experiments as previously described in detail [78,79]. The animals were housed in cages in standard laboratory conditions (a 12-h light/dark cycle, free access to food and water). All efforts were made to minimize the animals' suffering and the number of animals used. The animals were anesthetized with ketamine (50 mg/kg, i.p.) and xylazine (10 mg/kg, i.p.). Anesthesia was confirmed by the lack of paw withdrawal, whisker movement, and eye blink reflexes. The head skin was then removed, and the animal was implanted with a metal head-holding plate. After 2 days of recovery, the head-fixation training on a custom-made stereotaxic fixture was repeated for 1–3 h per day until the implanted animal learned to remain quiet. During and after each session, the animal was rewarded with free access to sucrose-containing water. During the final three sessions, sham experiments were conducted to habituate the animal to the experimental

conditions and noise. On the final 2–3 days, the animal was maintained virtually immobile, i.e., quiet but awake, for more than 2 h. After full habituation, the animals were anesthetized with ketamine/xylazine. A craniotomy ($1 \times 1 \text{ mm}^2$), centered at 3.5 mm posterior to the bregma and 2.0 mm ventrolateral to the sagittal suture, was performed, and the dura was surgically removed. The exposed cortical surface was covered with 1.7–2.0% agar at a thickness of 0.5 mm. Throughout the experiments, a heating pad maintained the rectal temperature at 37°C , and 0.2% lidocaine was applied to the surgical region for analgesia. For patch-clamp recordings, the recorded area was confirmed by post-hoc imaging of the intracellularly loaded Alexa 594, which was dissolved at $50 \mu\text{M}$ in patch-clamp solution. For calcium imaging, pressure-injected SR101, which was dissolved at 0.1 mM in Fura 2-containing solution, was imaged post-hoc to confirm the recorded area. Recordings were initiated after recovery from anesthesia, which was confirmed by spontaneous whisker movements and touch-induced eye blink reflexes. The total periods of recording were restricted to less than 1 h to minimize stress in the animals.

Visual stimulation

Visual stimuli were generated in custom-written MATLAB routines (The MathWorks, Natick, MA, USA) with Psychtoolbox extensions. A 17-inch TN-LCD monitor (refresh rate = 60 Hz) was placed 30 cm away from the right cornea, so that it covered 38.8° horizontally and 29.6° vertically of the mouse visual field. For flash stimulation, sinusoidal gratings (spatial frequency: 0.16 cpd; temporal frequency: 2 Hz; contrast: 100%) were presented in four evenly spaced orientations (0° , 45° , 90° , and 135°). The flash duration was set to range between 17–50 ms. Measurement using a high-speed

CMOS camera (ORCA-Flash2.8, Hamamatsu, imaged at 2,000 Hz) revealed that a flashing light on the TN-LCD monitor decayed with a time constant $\tau_{1/2} = 5.5$ ms, and thus, the afterglow was virtually ignorable. For each orientation, the gratings were presented at 2–4 spatial phases, and the responses were averaged to remove the effects of spatial phases. Flash stimuli were intervened with a gray screen for intervals of 8–10 s. In each set, stimuli with four orientations were presented in a pseudo-random order, and the set was repeated 10–40 times. For drifting grating stimulation, sinusoidal gratings (spatial frequency: 0.12 cpd; temporal frequency: 2 Hz; contrast: 100%) moved toward eight evenly spaced directions (0° , 45° , 90° , 135° , 180° , 225° , 270° , and 315°) for 1.5 s at intervals of 8–10 s for electrophysiology and for 2 s at an interval of 6 s for calcium imaging. A gray screen was shown during the interval period. In each set, drifting stimuli with 8 directions were presented in a pseudo-random order, and the set was repeated 10–40 times. In the Flash+Drift trials, each flash stimulus was followed by a drifting grating stimulus at an SOA of 0.5 s. In Figure 16., the flash stimuli were fixed at the vertical orientation (0° , vFlash), whereas in Figure 17 the drifting gratings were fixed at the vertical orientation (0° , 180° , vDrift) and moved rightward or leftward.

Voltage-sensitive dye imaging

The procedures for in vivo voltage-sensitive dye imaging have been previously described in detail [33,80]. The dye RH-1692 (Optical Imaging, New York, NY) [81] was dissolved in 4-(2-hydroxyethyl)-1-piperazineethanesulphonic acid (HEPES)-buffered saline solution (0.6 mg ml^{-1}) and applied to the exposed cortex for 60–90 min, which stained all neocortical layers. Imaging was initiated approximately 30 min after washing the unbound dye. To minimize movement artifacts because of

respiration, the brain was covered with 1.5% agarose made in HEPES-buffered saline and sealed with a glass coverslip. For data collection, 12-bit images were captured at 6.67-ms temporal resolution with a charge-coupled device camera (1M60 Pantera, Dalsa, Waterloo, ON) and an EPIX E4DB frame grabber with XCAP 3.1 imaging software (EPIX, Inc., Buffalo Grove, IL). RH-1692 was excited with red LEDs (Luxeon K2, 627-nm center) and excitation filters of 630 ± 15 nm. Images were obtained with a microscope composed of front-to-front video lenses (8.6×8.6 mm field of view, $67 \mu\text{m}$ per pixel). The depth of field of our imaging setup was 1 mm. RH-1692 fluorescence was filtered through a 673-to-703-nm band-pass optical filter (Semrock, New York, NY). Visual responses were averaged from 40-80 trials of stimulus presentations. Responses to flashes were expressed as the percent change in RH-1692 fluorescence relative to the baseline fluorescence intensity ($\Delta F/F_0 \times 100\%$). Gating flashes were applied to the retina at a distance of approximately 10 cm from the cornea contralateral to the recording site to cover the entire optic angle. Stimulation was repeated every 10 s.

Electrophysiology

The signal was amplified with a MultiClamp 700B, analyzed with pCLAMP10.1 (Molecular Devices, Union City, CA, USA) and digitized at 20 kHz. The data were reduced to 2 kHz and off-line analyzed using custom-written MATLAB routines. Patch-clamp recordings were obtained from L2/3 neurons at depths of 150–350 μm from the V1 surface using borosilicate glass electrodes (3.5–6.5 M Ω) that were pulled with a P-97 puller (Sutter Instruments, Novato, CA, USA). The electrode tips were lowered perpendicularly into the V1 with a DMX-11 electric manipulator (Narishige, Tokyo, Japan) or obliquely (at 30°) with a PatchStar micromanipulator (Scientifica, Uckfield,

UK). For cell-attached recordings, pipettes were filled with aCSF. For whole-cell recordings, the intra-pipette solution consisted of the following (in mM): 130 K-gluconate, 10 KCl, 10 HEPES, 10 Na₂-phosphocreatine, 4 Mg-ATP, 0.3 Na₂GTP, 0.05 Alexa-594 hydrazide, and 0.2% biocytin, adjusted to pH 7.3. For morphological reconstruction of the recorded cells, mice were perfused transcardially with 4% paraformaldehyde, and their brains were coronally sectioned at a thickness of 200 μ m using a DTK-1500 vibratome (Dosaka, Kyoto, Japan). The sections were incubated with 0.3% H₂O₂ for 30 min and permeabilized with 0.2% Triton X-100 for 1 h. Then, the sections were processed with ABC reagent at 4°C overnight and developed with 0.0003% H₂O₂, 0.02% diaminobenzidine, and 10 mM (NH₄)₂Ni(SO₄)₂. Experiments in which the series resistance exceeded 70 M Ω or changed by more than 15% during the recording session were discarded. For each neuron, spike responses to a brief inward current were examined, and regular spiking neurons were selected as putative pyramidal cells for the subsequent analyses. LFPs were recorded at a depth of 300 μ m from the V1 surface, which corresponded to L2/3, using borosilicate glass pipettes (1–2 M Ω) filled with aCSF. Traces were band-pass filtered between 1 and 250 Hz.

Human EEG

Ten healthy adults (four males and six females, 25.9 ± 5.4 (mean \pm SD) years old) with normal or corrected-to-normal vision participated in our EEG experiments. The EEG experiment was conducted in a dark room to explore early and late components of the visually evoked ERPs for brief exposures to high-contrast grating stimulus flashes. Visual stimuli were generated on a computer using Psychophysics MATLAB toolbox [82]. The stimuli were presented using a gamma-corrected [83] LCD display (EIZO FlexScan

S2243W, EIZO corporation, Ishikawa, Japan) whose spatial resolutions were 1,920×1,200 pixels, and the refresh rate was 60 Hz. Participants viewed the stimuli at a 55-cm distance from the display. The experiment contained two stimulus conditions (vertical and horizontal gratings), and the EEG signals for each of the stimuli were acquired 200 times (100 for the horizontal grating and 100 for the vertical grating). In each trial, the start of the trial was informed by the change of the color of the central fixation point (from gray to white). After 3-4 s (randomly jittered to exclude participant's expectation effect on the EEG signals) of the fixation color change, a high-contrast (100% from the gray background) gray-scale sinusoidal grating (1.03 cycles per degree) pattern (35.2×24.4° in visual angle) was flashed for 50 ms. The background brightness was 17.80 cd/m², which corresponds roughly to 4.88 lux, and the grating brightness ranged from 0.26 cd/m² (0.07 lux) to 35.62 cd/m² (9.77 lux). Then, participants were asked to keep fixating the central fixation for 4 s without blinking as much as possible. After the 4-s fixation period, the central fixation color changed from white to gray to inform the end of a trial. The task start was initiated by a button press by a participant. The participants could take breaks between trials as they liked, and they could proceed the experiments at their own paces. The stimulus presentation order was pseudo-randomized for each participant. One EEG session took about 2 h. The human visual ERPs at O1 and O2 (following the international 10/20 coordinate convention) for the two stimulus configurations were collected at 1 kHz (the left earlobe was used as a reference) with a wireless EEG system (Polymate Mini AP108, Miyuki Giken Co., Ltd, Tokyo, Japan) with paste-less dry electrodes (National Institute of Information and Communications Technology, Japan) [84]. Electrode impedances for O1 and O2 were kept below 5kΩ at the beginning of the measurements. Eye-movements and blinks were simultaneously

recorded with an electrode put on a left eye lid. The onset of the visual stimulus presentation and the EEG measurements were synchronized using a customized photo-trigger detection system (C6386, Hamamatsu Photonics K.K., Shizuoka, Japan). The recorded EEG and eye blink-related signals were saved on a computer using in-house MATLAB subroutines after each trial through a Bluetooth wireless connection. The ERP time series were analyzed using EEGLAB MATLAB toolbox ([85], <http://sccn.ucsd.edu/eeglab/>) and in-house subroutines written in MATLAB. The EEG signals were aligned off-line so that we could evaluate the time series from -200 ms to 3,000 ms relative to the grating stimulus onset. The raw data were preprocessed off-line by a linear trend removal and a band-pass filtering (0.5 to 100 Hz). Additionally, EEG epochs that contained large potentials exceeding the threshold (40 μ V) and abnormal spike or drifting components were excluded by EEGLAB's automatic outlier detection utilities and visual inspections. These noisy epochs were generally derived from eye-movements and blinks. The signal amplitudes were re-computed carefully by taking the mean of -200 to 0 ms (relative to the stimulus onset) samples as the baseline for each epoch. The recorded signals from two electrodes were similar and hence averaged for each participant. Finally, the ERPs averaged over 10 participants were given as the final visual event-related time series. The statistical tests to explore whether the signals were higher or lower than the baseline were evaluated by the standard two-tailed t -test at each sampling point ($P < 0.05$ without corrections of multiple-comparisons).

OSI and tuning curve

The OSI was defined according to the following equation:

$$OSI = \frac{\sqrt{(\sum R_{\theta} \sin 2\theta)^2 + (\sum R_{\theta} \cos 2\theta)^2}}{\sum R_{\theta}}$$

where R_θ is the mean response amplitude to a grating with direction θ [86]. Note that this equation defines the normalized norm of the averaged vector [86] and may give a value that is different from OSI used in other reports [41]. The similarity of the tunings curves between the early and late responses was evaluated using the correlation coefficient (R) of the amplitudes of the responses:

$$R = \frac{\sum(R_{\theta_early} - \bar{R}_{\theta_early}) \sum(R_{\theta_late} - \bar{R}_{\theta_late})}{\sqrt{\sum(R_{\theta_early} - \bar{R}_{\theta_early})^2} \sqrt{\sum(R_{\theta_late} - \bar{R}_{\theta_late})^2}}$$

where R_{θ_early} and R_{θ_late} are the amplitudes of early and late responses, respectively, to a grating with direction θ . \bar{R}_{θ_early} and \bar{R}_{θ_late} represent the mean of the response amplitudes R_{θ_early} and R_{θ_late} across all eight θ s. For each cell, the OSI and R were compared with their chance levels, which were estimated using a conventional random resampling method in which 1,000 surrogates were generated by randomly shuffling all trials irrespective of θ .

Two-photon calcium imaging

The mouse was placed in a stereotaxic frame and then on the stage of an upright microscope (BX61WI; Olympus). Cortical neurons were loaded with Fura 2, a calcium-sensitive fluorescent dye, under online visual guidance with a two-photon laser scanning microscope (FV1000; Olympus). Fura 2 AM was dissolved at 10 mM in DMSO with 10% pluronic acid and diluted at the final concentration of 1 mM in aCSF that contained 0.1 mM SR101. This solution was pressure-injected (50–100 mbar for 10 s) into V1 at a depth of 150–250 μm from the surface through a glass pipette (tip diameter: 10–30 μm). The pipette was carefully withdrawn, and the craniotomized area was sealed with 2% agar and a glass cover slip. After 50–70 min, which enabled the dye loading to the neuronal soma and the washout of extracellular dyes, the Fura-2 fluorescence was two-photon imaged from V1 L2/3 neurons. Neurons and astrocytes were discriminated

based on astrocyte-specific staining with SR101 [87]. Fura 2 and SR101 were excited by a mode-locked Ti: sapphire laser at wavelengths of 800 nm and 910 nm, respectively (100 fs pulse width, 80 MHz pulse frequency; Maitai HP; Spectra Physics) [88]. Fluorescent light was corrected by a water-immersion objective lens (20×, numerical aperture 0.95; Olympus). Videos were taken from a 320×320- μm area at 5 frames per second using FV10-ASW software (version 3.0; Olympus). Neurons that exhibited significant visual responses above the baseline ($P < 0.05$, paired t -test) in any recording session were selected for analysis.

Virtual optomotor system

The apparatus was located in a dark, soundproofed room. The room temperature was maintained at 25°C during the experiment. A virtual cylinder comprising a vertical sinusoidal grating (0.17 cpd, 10–40% contrast) was displayed in three-dimensional coordinate space on four 24-inch monitors (refresh rate: 60 Hz) that were arranged in a quadrangle arena. The images on the monitors were extended by two mirrors on the top and bottom of the arena. A platform (a white acrylic disc; $\phi = 6.0$ cm) was positioned 13.5 cm above the bottom mirror. In each experiment, a single male P28–35 C57BL/6J mouse was placed on the platform and was allowed to move freely. The behavior of the mouse was monitored through a camera (Logicool HD Webcam C615; Logitech, Tokyo, Japan) that was attached over a small hole of the top mirror. Vertical gratings that drifted leftward or rightward (temporal frequency: 0.5 Hz) were presented simultaneously on all four screens for 2 s with a random interval between 2–4 s. From the animal's point of view, the virtual cylinder appeared to rotate around the platform at an angular velocity of 5° per second). The mice normally tracked the grating with reflexive head

movements in concert with the rotation direction. The drifting directions were randomly alternated, and the rotations were repeated 120 times in one session that took approximately 10 min. In some trials, either a vertical or horizontal grating (0.17 cycles per degree, 100% contrast) was flashed 0.5 or 3 s before a drifting grating. Animals were habituated to the system prior to the first behavioral test by experiencing at least one full session. When the mice slipped or jumped down from the platform during the test, they were manually returned to the platform, and the test was resumed. If the animal's head evidently tracked a cylinder rotation, the trial was counted as a 'success'. Manual counting was checked by two independent trained researchers who were blind to the experimental conditions. Through computer-generated order randomization of the stimulation conditions, the experimenters were also blind to the treatment. The trials in which a mouse was grooming or made large movements were excluded from the analyses (invalid trials). The success rate was calculated as a ratio of the successful trials to the total valid trials. Tetrodotoxin was dissolved at 10 μ M in aCSF and directly applied to the cortical surface 15 min prior to the behavioral sessions. The exposed cortices were covered with the craniotomized bone segments and mounted with dental cement. The effects of tetrodotoxin were confirmed by flash-induced LFP responses in V1 L2/3.

Human psychophysics

Eleven healthy right-handed individuals (3 females) with normal or corrected-to-normal vision participated. The ages ranged from 22 to 42 years, with 26.5 ± 5.1 years (mean \pm SD). The participants performed tasks using a computer mouse with their right hands. A 24-inch monitor was placed at a distance of 0.5 m from the participants' eyes in a dark,

pseudo-soundproofed room. The participants were instructed to report the motion direction of drifting gratings presented on the screen. A 2×2 cm² open square was displayed at the center of the screen against a gray background (60 cd/m², 5 lux). Each trial was initiated when a participant clicked the computer mouse on the square. Then, the square was filled in black, and after a random time interval between 1–3 s, a sinusoidal drifting grating (spatial frequency: 0.12 cpd; temporal frequency: 1 Hz; contrast: 40%) was presented for 0.25 s in one of four movement directions (0°, 90°, 180°, and 270°). A 50-ms beep tone was presented 0.5 s before a drifting grating stimulus. In some trials, a 50-ms grating flash (spatial frequency: 0.12 cpd; contrast: 100%) was displayed simultaneously with the tone. A full gray screen was displayed during all inter-stimulus intervals. After each stimulus, the participants were asked to move the mouse cursor in the same direction as the grating motion as rapidly as possible. When the mouse cursor traversed the edge of the square, the square became blank, which cued the trial completion. Incorrect motion reports or failures to respond within 600 ms (misses) from stimulus onset were considered errors and were indicated to the participants through a 200-ms peep tone. Each participant performed 160–244 trials per session.

RESULTS

V1 late responses

We monitored the spiking activity of V1 layer (L) 2/3 neurons of P35-44 mice using the cell-attached recording technique (Fig. 1A) and applied a brief flashing stimulus (17–50 ms) of a full-field gray-scale sinusoidal grating with one of four orientations (0, 45, 90, and 135°) to the eye contralateral to the recording site. As previous reports have demonstrated that L2/3 neurons fire sparsely [26-30], 56.5% of V1 neurons (43 of 76 cells) exhibited a significant increase in their firing rates in response to the grating flashes (defined by a criterion of $P < 0.05$ versus the baseline firing rates, Z-test for comparison of two counts [31]). The responses were classified into two types; the first type of responses was spikes immediately (< 0.3 s) after the stimulus onset (early spiking, Fig. 1A top), whereas the second type was spikes with latencies longer than 0.4 s (late spiking, Fig. 1A bottom). In the pooled data, the population firing rates exhibited two distinct peaks that corresponded to the first and second types of spikes; for individual responsive neurons, the mean firing rates during the early and late responses were 1.27 ± 0.91 Hz and 0.28 ± 0.19 Hz, respectively (mean \pm SD of 11 and 36 neurons). Late spiking neurons were numerically dominant (Fig. 1B, inset). Thus, we defined the early and late responses as activity that occurred between 0–0.3 s and 0.4–2 s, respectively.

To investigate the subthreshold V_m dynamics that underlie the biphasic spike responses, we conducted whole-cell current-clamp ($I = 0$) recordings from V1 neurons (Fig. 2A-C). In the typical neuron shown in Fig. 2B, a grating flash reliably induced early and late depolarization responses. Remarkably, we observed similar biphasic V_m responses in all 28 recorded neurons (Fig. 3A, B), irrespective of their firing types, including non-spiking neurons (Fig. 3C). The early depolarization was transient and

peaked at latencies of < 0.3 s, whereas the late depolarization was more persistent and peaked at approximately 0.4–2.0 s. On average, the peak amplitudes of the early and late depolarizations were 6.7 ± 4.2 and 6.4 ± 4.4 mV (mean \pm SD of 28 cells), respectively, and were correlated with each other (Fig. 3B left). The area under curves of individual V_m traces during a late period of 0.4–2.0 s (late area) was correlated with their peak amplitudes (Fig. 3B middle). Therefore, we quantified both early and late responses using their peak amplitudes in the following analyses. The areas of late responses were not correlated with their peak latencies (Fig. 3B right). Thus, the latencies did not affect the magnitude of late responses. This fact also validates our choice of the time window for late V_m responses (0.4–2.0 s).

The fact that late depolarizations occurred in all recorded neurons suggests that late visual responses represent a global phenomenon that involves the entire V1 cortex. To confirm this possibility, we recorded local field potentials (LFPs), which reflect the compound activity of multiple neurons surrounding the tip of a recording electrode [32]. We found that LFPs in V1 L2/3 responded reliably to a grating flash with biphasic negative fluctuations (Fig. 4). The response signal was, if any, less evident in LFPs recorded from the retrosplenial cortex, a more anterior brain region. We also recorded voltage dynamics of the neocortical surface. We loaded the cerebral surface with RH-1692, a voltage-sensitive dye (VSD), and monitored the spatiotemporal patterns of flash-evoked activity [33]. As expected by the LFP data, early cortical VSD responses were observed in V1 (Fig. 5). Then, the VSD signal decreased transiently, producing a transitional period. After approximately 0.4 s, the late VSD responses also arose at V1. Therefore, similar to V_m responses in patch-clamp recordings, the VSD signal in V1 was biphasic. We extended the field potential work to visual responses in humans. We

recorded EEG from 10 adult participants and measured visual event-related potentials (ERPs) at O1 and O2, according to the international 10/20 coordinate convention [34]. Human ERPs in response to grating flashes were also biphasic; an early and late negative reflection peaked around 0.15 s and 0.7 s, respectively, after a grating flash (Fig. 6).

Previous studies have also reported a specific form of late, slow activation of the rat V1 [4,5] and the mouse primary somatosensory cortex [35]; however, these responses emerged as a result of sensory reinforcement learning and were not observed in naïve animals. There is also a study that has reported biphasic responses in naïve cat visual cortex [36]; however, the latency and the duration of this late response was much shorter. By contrast, our flash-evoked late V1 responses occurred in naïve animals and had a much longer latency and duration. Therefore, they represent novel V1 dynamics. This discrepancy most likely occurs as a result of the difference in the features of visual stimuli. Indeed, the durations of flashes were critical [7]; we failed to observe evident long-delayed LFP activity at flash durations of more than 200 ms (Fig. 7). Moreover, we used full-field flashes, which might recruit synaptic inputs from both classical and non-classical visual receptive fields. It should also be noted that flash-induced late response has much a longer duration than the well-known OFF response that have been described in other studies [37].

Orientation selectivity of late V1 response

The amplitudes of both early and late responses increased at higher contrasts of flash gratings (Fig. 8). Thus, it is feasible that the late responses encode the orientation of flashing stimuli [36]. We measured the orientation selectivity, which is a characteristic of V1 neuron responses [38-41]. Grating flashes with various orientations induced different

changes in the late spike rates (Fig. 9A). We calculated the orientation selectivity index (OSI) for each late-spiking neuron. On average, the OSIs were 0.37 ± 0.25 (mean \pm SD of 36 cells). To evaluate the statistical significance of OSIs, we compared them with the chance distribution obtained from the trial-shuffled surrogate data (Fig. 9B). Overall, the OSIs exhibited significantly higher values than chance, which indicates that the late spiking responses were orientation-selective ($P = 3.3 \times 10^{-3}$, $D = 0.29$, $n = 36$ cells, Kolmogorov-Smirnov test). Late subthreshold V_m responses were also significantly orientation-selective (Fig. 10, $P = 2.7 \times 10^{-9}$, $D = 0.66$, $n = 34$ cells, Kolmogorov-Smirnov test). Their OSIs were lower compared with the late spike responses (Fig. 11, $P = 5.0 \times 10^{-3}$, $t_{19} = 3.17$, $n = 20$ cells, paired t -test), consistent with many previous reports about orientation selectivity of V_m responses [42-44].

Because the early responses were also orientation-selective, we focused on the tuning properties of the early and late responses. We computed the correlation coefficients between the early and late V_m tuning curves of each cell and compared the pooled data to the chance-level distribution of the correlation coefficients in their trial-shuffled surrogates. The correlation coefficients were significantly higher compared with chance, which indicates that the early and late V_m responses of each neuron had a similar orientation tuning (Fig. 12A, $P = 0.014$, $D = 0.27$, $n = 34$ cells, Kolmogorov-Smirnov test). Moreover, the OSIs of late responses were positively correlated with the OSIs of early responses (Fig. 12B, $R^2 = 0.61$, $P = 1.2 \times 10^{-4}$, $t_{17} = 4.94$, t -test for a correlation coefficient). Note that neither early nor late OSIs depended on firing rates (Fig. 13, $P = 0.490$, $R^2 = 0.01$). We thus conclude that late responses conveyed selective information of visual stimuli.

We further confirmed flash-induced responses using two-photon calcium imaging. We loaded V1 L2/3 neurons with Fura 2 by pressure-applying its acetoxymethyl ester (AM) derivative (Fig. 14A). The amplitude of a spike-elicited calcium elevation ($|\Delta F/F|$) was nearly linear with the number of action potentials involved in the calcium event (Fig. 14B). Note that our imaging system was able to resolve two action potentials at an inter-spike interval of less than 400 ms (Fig. 14C), allowing us to classify early and late spiking neurons. We imaged spike-triggered calcium events *en masse* from 64.6 ± 6.04 neurons per video (mean \pm SD of 9 videos from 9 mice) with a single-cell resolution at 5 frames per second (Fig. 15A). In the example neuron shown in Fig. 15B, the amplitudes of the $\Delta F/F$ responses evoked by grating flashes exhibited orientation selectivity. Of the 581 neurons, 323 (56%) neurons were responsive to flashes, and the preferred orientations were uniformly distributed (Fig. 15C). Because early spiking responses occurred around 0.1-0.2 s after a flash, they would be reflected in a rapid $\Delta F/F$ increase in the first video frame (0.2 s) after the stimulus. According to this definition, we estimated that early spiking neurons contributed 10.0% (58 out of a total of 581 cells), consistent with patch-clamp recording data showing that the majority of flash-responsive neurons are of the late-spiking type (Fig. 1B inset and Fig. 3C). Therefore, we assumed that most $\Delta F/F$ responses reflected putatively late spikes. Although they may overlap with the early-spiking component, the orientation tuning properties were approximately congruent between the early and late responses (see Fig. 12A), and thus, the $\Delta F/F$ response tuning is still thought to reflect the late spiking tunings. Consistent with this notion, the distribution of OSIs in the $\Delta F/F$ responses was similar to the late-spiking responses obtained by patch-clamp recordings

(Fig. 15D, $P = 0.497$, $D = 0.15$, Kolmogorov-Smirnov test) and was higher than that of their surrogate data ($P = 2.3 \times 10^{-6}$, $D = 0.15$, $n = 323$ cells).

Flash-modulated V1 response

Because the late response has a long latency, it may interact with a subsequent visual stimulus. We tested this idea by recording the $\Delta F/F$ responses to grating stimuli that moved for 2 s toward one of eight directions (0° , 45° , 90° , 135° , 180° , 225° , 270° , and 315°), which were presented alone (Drift-only trials) or 0.5 s after grating flashes (Flash+Drift trials). To minimize photobleaching and phototoxicity, we did not test all possible combinations of the flash orientations and the drifting grating directions; instead, we fixed the grating flash orientation to 0° (vertical orientation; vFlash) and reduced the total imaging period (Fig. 16A). We compared the $\Delta F/F$ responses between Flash+Drift and Drift-only trials and examined how the preceding vFlash (prime) modulated the $\Delta F/F$ responses to subsequent drifting gratings (target). The combinational pattern of a vFlash stimulus and a drifting grating was described as a Δ orientation, which represents the orientation difference between vFlash and the drifting gratings and comprised a value of -45° , 0° , 45° , or 90° ($= -90^\circ$). In Drift-only trials, Δ orientation indicates the difference between 0° and the orientations of drifting gratings (*i.e.*, the absolute orientation).

Fig. 16B summarizes the data from a representative neuron. For each Δ orientation in Drift-only and Flash+Drift trials, we statistically judged whether the neuron responded, *i.e.*, whether the $\Delta F/F$ amplitude was significantly higher compared with the baseline $\Delta F/F$ fluctuation ($P < 0.05$, $n = 10$ – 18 trials, paired t -test). The significant responses are marked by dark red boxes below the tuning plot. Three other examples are

shown in Fig. 16C. We pooled the data from the 581 neurons (Fig. 16D). For each Δ orientation, we compared the number of cells that exhibited significant $\Delta F/F$ in Drift-only trials to the number of significant cells in Flash+Drift trials. Notably, the number of significantly responsive cells increased at Δ orientation = 0° , where the orientations of vFlash and drifting gratings were matched. The number of responsive cells did not increase at the other Δ orientations. Thus, two sequential stimuli with the same orientation activated V1 neurons more efficiently compared with stimuli with different orientations. By focusing on individual cells that were activated under the iso-orientation condition, we analyzed their intrinsic orientation preferences. Flash-induced response enhancement was more evident in cells whose preferred orientations were different from the stimulus orientation (Fig. 16E). These data indicate that a flash recruited otherwise irresponsive cells (due to their cross-orientation preferences) to a subsequent stimulus with the same orientation as the flash.

Previous studies have reported that paired visual stimuli lead to a functional adaptation of neuronal responses to the target [45,46]. In other words, visual cortical neurons decrease their responsiveness to repeated stimuli. Calcium imaging did not allow us to strictly quantify the response amplitude, and we could not determine whether the observed changes are adaptation (desensitization) or priming (sensitization). To quantify the effect of flashes in more details, we returned to patch-clamp recordings of subthreshold V_m responses. In these experiments, the drifting grating orientation was fixed to vertical (0° , 180° ; vDrift), and the orientations of the preceding flashes varied across four orientations (0° , 45° , 90° , or 135°) in a pseudo-random order (Fig. 17A). First, the SOA was set to be 0.5 s (Fig. 17B). We compared the amplitudes of V_m responses to a combination of flash and vDrift stimuli (Flash+vDrift) with those of the

responses to vDrift alone (vDrift-only). On average, the absolute amplitudes of Flash+vDrift responses were larger than those to vDrift-only responses ($P = 0.012$, $t_{51} = 2.60$, paired t -test); however, for individual neurons, the amplitude relations depended on the amplitudes to responses to Flash alone (Flash-only, Fig. 17C). That is, when a neuron exhibited a large depolarization in Flash-only trials (> 2 mV), then the depolarization in Flash+vDrift trials was more increased compared to vDrift-only responses. On the other hand, when a neuron exhibited a small depolarization in Flash-only trials (< 2 mV), the Flash+vDrift response amplitude was nearly comparable to the vDrift-only response amplitude. To further examine this effect, we employed a new analysis in which we compared Flash+vDrift responses with the linear summation of the Flash-only response and the vDrift-only response (Fig. 17D). We found that this augmentation occurred below the value of simple arithmetic summation of two responses. That is, individual responses to Flash-only and vDrift-only stimuli were sublinearly integrated in Flash+vDrift trials (Fig. 17D). In our experimental conditions, therefore, a flash facilitated the vDrift responses through a sublinear integration of V_m depolarizations. Notably, their sublinearity differed depending on the orientations of flash gratings and was smaller at $\Delta\text{orientation} = 0^\circ$ than at 90° (Fig. 17D). In other words, when two orientations of flash gratings and drifting gratings were matched, the combined responses were less sublinear, thereby exhibiting apparently larger response amplitudes, which is consistent with the flash-induced enhancement in the calcium imaging experiments. This $\Delta\text{orientation}$ -dependent difference was not found at SOAs of 0.05 or 3 s (Fig. 17D), suggesting the involvement of the orientation selectivity of flash-induced late responses. We re-plotted these sublinear behaviors (SOA = 0.5 s) as a function of the difference between their intrinsic orientation preferences and the

orientation of the grating stimuli. Flashed-induced response sublinearity was the largest in cells whose preferred orientations were identical to the stimulus orientation (Fig. 17E). This was also consistent with the results in calcium imaging.

Flash-modulated visual perception

Flash-induced modulation of V1 neuronal activity prompted us to evaluate its behavioral consequences. We first measured the visual performance of mice using a virtual optomotor test, which can assess the visual detection ability of naïve mice without behavioral training [47]. A freely moving mouse was placed on the circular platform surrounded by four computer screens on which vertically orientated gratings moved leftward or rightward for 2 s (Fig. 18A; vDrift). As a visuomotor reflex, the mouse turned its head in the same direction as the vDrift movement, a behavior that is called a tracking response. The ratio of trials with the tracking responses to the total trials was calculated as the tracking rate and was used as a quantitative measure of visual function. Under the baseline conditions (*i.e.*, vDrift-only trials), the mean tracking rate was $74 \pm 13\%$ (mean \pm SD of 10 mice). This ratio increased to $86 \pm 10\%$ when vertical flashes were presented 0.5 s before vDrift (Fig. 18B, Δ orientation = 0° ; $P = 0.037$, $t_9 = 2.45$, paired *t*-test). This increment was not observed when horizontal flashes (Δ orientation = 90°) were coupled (Fig. 18B; $P = 0.92$, $t_9 = 0.10$) or when vertical flashes were presented at an SOA of 3 s (Fig. 18C; $P = 0.69$, $t_{10} = 0.41$). In mice that received local injection of 10 μ M tetrodotoxin into the V1, flash-induced responses in V1 LFP disappeared (Fig. 19A). In these mice, the tracking rate for the vDrift-only trials was reduced to $18 \pm 16\%$ ($n = 4$ mice, $P = 0.026$ versus naïve mice, $t_3 = 4.13$, Student's *t*-test) and was not increased by

vertical flashes (Fig. 19B). Thus, flash-induced increases in the tracking rates likely depend on V1 late responses.

Finally, we conducted a psychophysical test in humans. The participants were asked to report the motion directions of 0.25-s drifting gratings (0° , 90° , 180° , or 270°) by flicking a computer mouse toward the same direction within 0.70 s (Fig. 20A). In Flash+Drift trials, grating flashings at orientations of 0° , 45° , 90° , or 135° were presented 0.5 s before the drifting gratings. The correct response ratio was approximately 100% and was not modulated by grating flashes with either Δ orientation (Fig. 20B; $P > 0.05$, $n = 11$ humans, $n = 486$ – 500 trials each, Student's t -test). However, the latency of the flicking response was significantly shortened at Δ orientation = 0 (Fig. 20C; Drift-only: 357.3 ± 54.6 ms *versus* 0° : 347.8 ± 56.0 ms, mean \pm SD; $P = 0.007$, $t_{993} = 2.71$). We did not think that this effect was due to illusory motion perception, because the grating phase of a flash stimulus and the first frame of the following drifting stimulus were identical. However, to examine the possible involvement of motion illusion, we presented two successive flashes at an SOA of 0.5 s with various combinations of the grating phases and asked participants to answer the "felt" motion direction (Fig. 21). Each stimulus condition was repeated for 80 times. As a result, the participants were not able to distinguish the motion direction; the responses were approximately 50% (= the chance level). Thus, two consecutive grating stimuli at an SOA of 0.5 s *per se* did not induce a motion perception.

DISCUSSION

We discovered that a brief flashing light evokes long-delayed, slow activation of the mouse V1 network. The late response was observed using different techniques, including patch-clamp recording, LFP recording, VSD recording, and EEG recording, which exclude the possibility of our recording artifact. Importantly, the late response actively interacted with subsequent visual input. This novel phenomenon was heretofore overlooked, probably because past studies tended to record visual responses for shorter terms (up to a few hundreds of milliseconds) than our work and because we used a short flash of full-field gratings, a stimulus pattern that is not very common in vision research. Another reason for the overlook of the late responses may be a consensus that visual responses occur within a few hundred milliseconds after the onset of the visual stimulus, which might have prevented an attempt to record visual responses for seconds.

There are mainly three candidates for the initiation site of the late response. First, the late activation of V1 circuit might be generated through reverberation of the recurrent circuit within the V1. Theoretically, cortical activity is sustained by local reverberation within a recurrent network [15,16]. Anatomically, L2/3 is enriched with horizontal synaptic connections [48,49] and provides the structural basis of a recurrent circuit. Although V1 L2/3 neurons receive synaptic inputs with various orientation preferences [50], the synaptic connection probability is biased toward a similar orientation preference [51,52]. Recent studies have demonstrated that neurons derived from the same precursor cells are more likely connected and share the same orientation preference [53-55]. These observations suggest the existence of fine-scale subnetworks dedicated to process specific information [56]. We determined that the tuning properties were significantly correlated between the early and late responses. Hence, the neuron

population activated by a grating flash is preferentially reactivated at the late phase. The visual cortex may filter visual input information through its specifically wired, reverberatory network [57] and may offer a high orientation tuning during the late response. The second possibility is that the V1 rebound activity arose from subcortical regions, including the lateral geniculate thalamus and the superior colliculus (and even the retina). The lateral geniculate thalamus is anatomically eligible for generating rebound activation, because it contains a recurrent network and receives feedback projections from V1 [37,58]. This anatomy might have led to the reliable observation of late response even in the LFP recording. Finally, top-down inputs from higher order cortices may also have the ability to induce late responses, as recently reported in the hindlimb somatosensory cortex [59]. However, the latency of the late response in the visual cortex was much longer than that observed in the study, suggesting a more complex mechanism than a simple top-down feedback process.

We speculate that reverberatory activity in V1 recurrent circuits admixes with late-coming feed forward V1 activity. Recent studies have demonstrated that co-stimulation of the thalamocortical and cortical pathways efficiently depolarizes cortical neurons through nonlinear summation [60,61]. Although a single L2/3 neuron receives variously tuned synaptic inputs irrespective of the orientation preference in the cell's spike output [50], synaptic inputs over dendritic trees are non-randomly distributed and are often spatially clustered [62-64]. Thus, synaptic inputs from flashing and drifting gratings may be locally converged and may lead to nonlinear dendritic boost [61,65] when two orientations are matched.

At the network level, a grating flash enhanced (or sublinearly integrated) the V1 responses to subsequent drifting gratings in an orientation-selective manner. In these

experiments, we used an SOA of 0.5 so that drifting gratings arrived during the period of flash-evoked late responses. Calcium $\Delta F/F$ responses to the drifting gratings were enhanced only when their orientations were identical to the preceding flashes. The flash-induced facilitation can be explained by two possibilities. First, the priming effect may facilitate the responses to sequential stimuli [66,67]. However, flash-induced response enhancement is not a normal form of priming because it was not a simple mixture of membrane potential depolarizations. Flash-induced late response and the response to drifting grating were integrated in a sublinear fashion, but more linearly at $\Delta\text{orientation} = 0^\circ$, suggestive of the partial existence of priming. It also differed depending on preferred orientations of the neurons. The second possibility is that the facilitation occurred through top-down neural processing [68], especially feature-based attention [69,70]. It is well known that attention modulates the responsiveness of neurons that have receptive fields within the attentional loci [71-73], enhancing task performance on late-coming target stimuli [70,74]. Moreover, it is important to note that feature attention in humans is effective at an SOA of approximately 0.5 s [69], consistent with our findings. Developing a psychophysical method to measure the attentional effect in mice may help verify the second possibility. Focusing on individual neurons and their orientation preferences, a flash recruited neurons with shifted-orientation preferences at the $\Delta\text{orientation} = 0^\circ$ condition. In other words, neurons with cross-orientated preferences to the flash orientation were less subject to the sublinearity when the responses were integrated. Consistent with this notion, at $\Delta\text{orientation} = 90^\circ$, neurons with cross-orientated preferences to a flash (i.e., iso-orientated with regard to the orientation of the drifting stimulus) exhibited the minimal sublinear property. Thus, flash-induced late responses might function to recruit

neurons that are otherwise irresponsive, leading to stronger activation of the primary visual cortex.

We found that ongoing visual processing and perception were both affected by the immediately preceding visual information in a feature-specific manner; however, we could not directly show the causal contribution of flash-induced delayed depolarizations per se to subsequent visual perception. Optogenetic prevention of the delayed responses [35] is not applicable to our cases; that is, even if optogenetic manipulation is performed only during the delayed activity period, it inevitably affects both flash-induced delayed responses and drifting grating-evoked activity and cannot isolate the effect of the flash responses on visual perception. Therefore, we need to seek a way to specifically diminish the delayed activity without affecting drifting-grating-evoked activity.

In this study, we regarded the featured flashes as a model of the initial visual scenes and aimed to separate the effect of suddenly coming and subsequently continuing visual scenes. Hence, we think that, under natural conditions, the pattern-selective late responses observed here may work to facilitate the responses to the passing object, possibly linking our findings to studies on trans-saccadic integration [75-77]. However, two major concerns remain unresolved. First, the late response occurred to flashes with durations of less than 50 ms, whereas natural saccades usually last about 300 ms. Thus, we cannot rule out the possibility that the late response we found is involved in other visual processes than trans-saccadic integrations. Second, although we obtained the behavioral correlates of flash-induced effects on visual function, flashes recruited neurons that were otherwise irresponsive because of the non-preferred orientation. Therefore, flashes may increase the overall activity level of V1 and diminish the selective responsiveness of individual neurons. According to this notion, the facilitation

of V1 activity would decrease the discrimination acuity of the animal, but at the same time, it could increase the sensitivity per se by lowering the visual detection threshold. This possibility must be clarified using a new behavioral paradigm that can distinguish visual detection from visual discrimination.

Chapter 1 of this doctoral thesis is published in the academic paper below:

Funayama K, Minamisawa G, Matsumoto N, Ban H, Chan AW, Matsuki N, Murphy TH, Ikegaya Y. Neocortical Rebound Depolarization Enhances Visual Perception. *PLoS Biol.* 2015; 13:e100223.

FIGURES

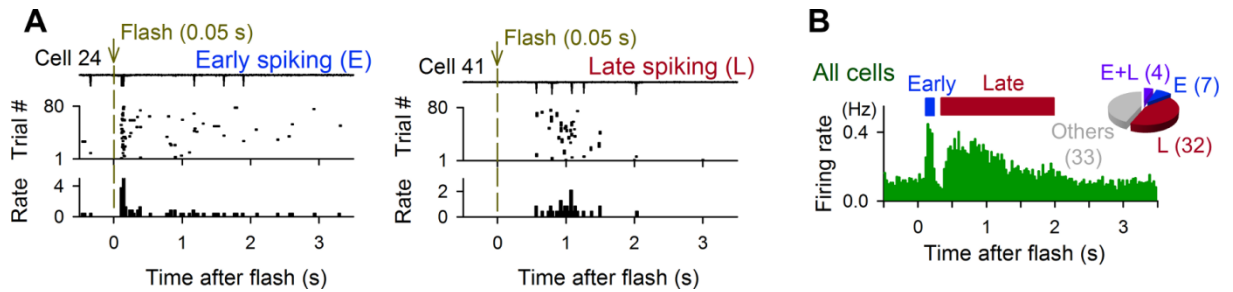


Figure 1. Flash-evoked biphasic spike responses in mouse V1 neurons. Cell-attached recordings were acquired from V1 L2/3 neurons in awake, head-restricted mice, whose contralateral eyes were presented 0.05-s full-field grating flashes at pseudo-random intervals of 8–10 s for 80-200 trials. (A) Raw traces of cell-attached recordings at 10 consecutive trials, the spike raster plots of the 80 trials and their peri-flash time histograms of the firing rates for two typical neurons. Cell 24 fired action potentials with short latencies, whereas cell #41 fired action potentials with longer latencies. (B) Data from 76 cells from 58 mice are pooled. The inset pie chart indicates the distribution of cells with early spiking (E), late spiking (L), and no activity change (others).

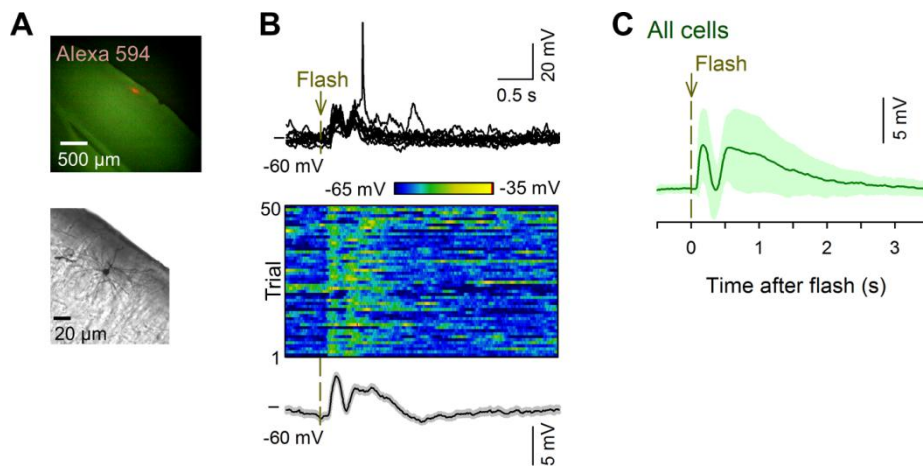


Figure 2. Flash-evoked biphasic subthreshold responses in mouse V1 neurons.

Whole-cell recordings were acquired from V1 L2/3 neurons in awake, head-restricted mice, whose contralateral eyes were presented 0.05-s full-field grating flashes at pseudo-random intervals of 8–10 s for 80–200 trials. (A) The top photo shows a coronal slice indicating the recorded site marked by pressure application of Alexa 594 loaded in the patch pipette, which corresponds to the V1 monocular region. The bottom photo shows post-hoc reconstruction of a whole-cell recorded L2 pyramidal neuron with intracellular biocytin staining. (B) The top raw traces show V_m responses in 10 consecutive trials in a representative neuron. V_m responses for 50 trials in the same neuron (middle pseudocolored map) were averaged in the bottom trace. The gray area indicates the SEMs. (C) Mean \pm SD of the subthreshold V_m responses of 34 cells from 30 mice.

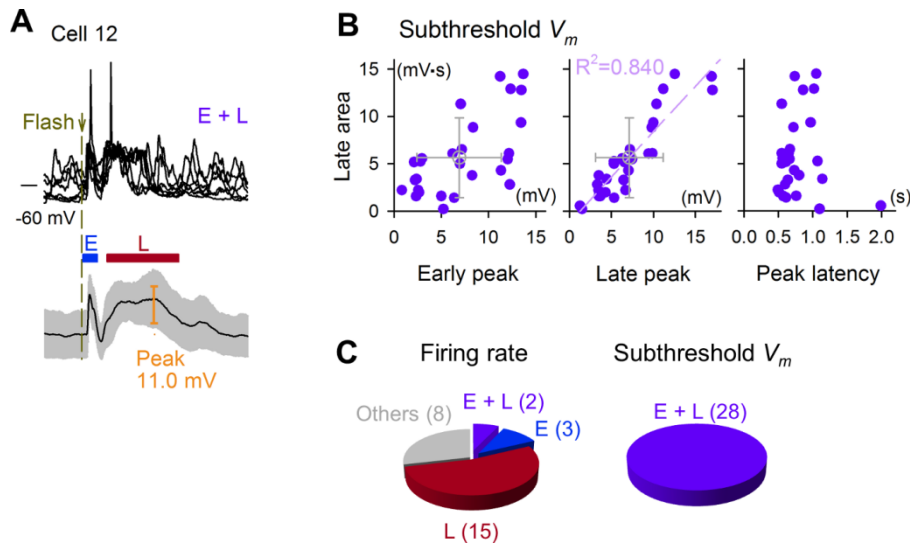


Figure 3. Early and late responses of V1 neurons

(A) V_m responses to 0.05-s full-field grating flashes were whole-cell recorded from V1 L2/3 neurons of awake mice. Raw traces at 10 consecutive trials (*top*) and the mean \pm SD (*bottom*) of the subthreshold V_m responses of cell #12 in 40 trials. The voltage response consisted of an early depolarization (E) that occurred earlier than 0.3 s after the stimulus onset and a late depolarization (L) that persisted up to 2 s and had a peak at approximately 0.4-2.0 s. (B) The area under curve of late depolarization was plotted against the peak amplitudes of the early (*left*) and late (*middle*) depolarizations and the peak latency of late depolarizations (*right*). Each purple circle indicates a single cell, and the gray symbols indicate the means \pm SDs of 28 neurons. The dashed line represents the best linear fit. All neurons exhibited significant early and late depolarizations ($P < 0.05$, paired t -test, calculated by the peak and mean amplitude, respectively, for the early and late response periods). (C) Pie charts indicate the distributions of cells classified as early responsive (E), late responsive (L), or early and late responsive (E + L), or the other non-responsive cells for spike (top) and subthreshold V_m responses (bottom). All recorded neurons ($n = 28$

cells) showed significant early and late subthreshold V_m responses (E + L), but their firing response types varied.

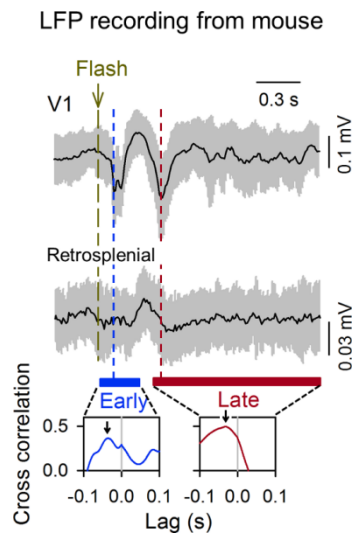


Figure 4. Biphasic responses of field potentials in mouse visual cortex to grating flashes. Local field potentials (LFPs) were recorded from L2/3 of the V1 and retrosplenial cortex, while a full-field grating flash was presented to the contralateral eye of an awake mouse. Two negative potentials appeared after a flash. The gray areas indicate the SDs. The arrows in the bottom cross-correlograms indicate the peak offsets, which show that early and late responses occurred earlier in V1 than in the retrosplenial cortex.

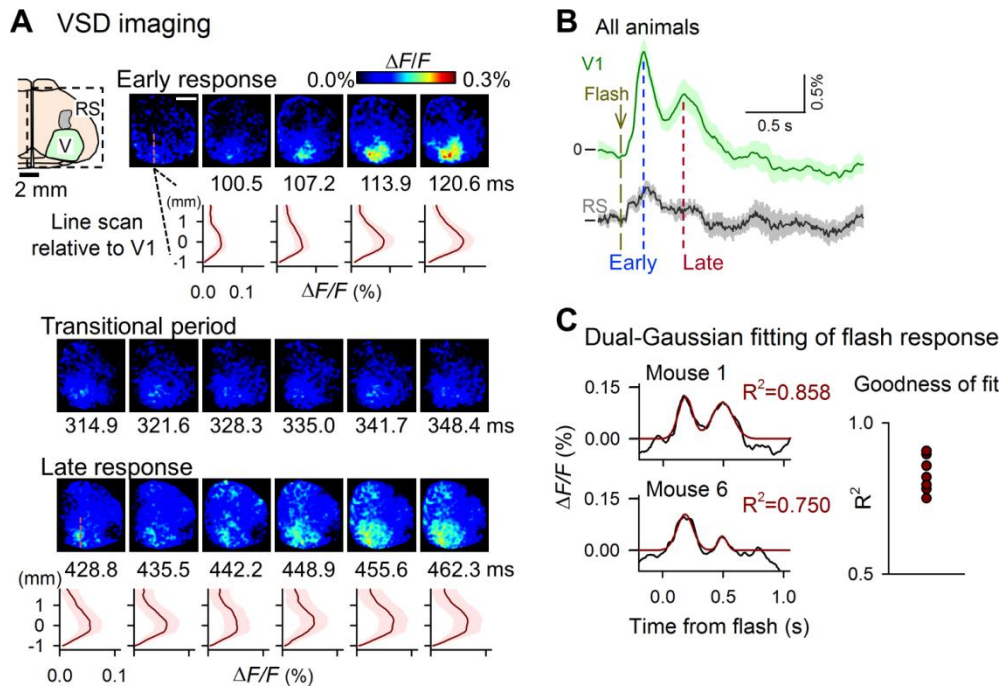


Figure 5. Spatiotemporal patterns of flash-evoked neocortical activity. VSD signal was time-lapse imaged from the right hemisphere, while a full-field grating flash was presented to the contralateral eye. (A) The top-left schematic indicates the cortical regions, including the V1. The snapshots indicate a time series of representative images at times indicated below. The bottom traces demonstrate the line-scanned VSD signal along the anterior-posterior axis of the cortex relative to V1, indicated in the red line in the top-left VSD image. Scale bar = 2 mm. (B) Mean \pm SEM of VSD signals in V1 and retrosplenial cortex (RS). $n = 8$ mice. (C) V1 VSD signals were fitted to dual Gaussian curves. Left: Two representative fittings. Right: In all 8 mice tested, R^2 exhibited $P < 0.01$.

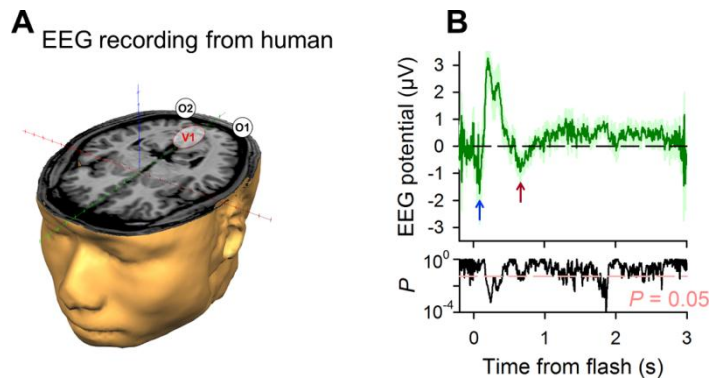


Figure 6. Biphasic responses of field potentials in human visual cortex to grating flashes. (A) Human electroencephalograms (EEGs) were recorded from O1 and O2, indicated in the left schematic. (B) Event-related potentials (ERPs) in responses to grating flashes are shown as mean \pm SD of 10 participants. The arrows indicate early and late negative potentials. The bottom plot represents the P values from the pre-stimulus baseline at the corresponding time points, indicating the presence of early and late responses.

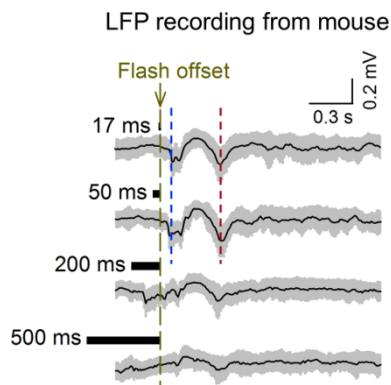


Figure 7. V1 late response is induced by flashes with short duration. Local field potentials (LFPs) were recorded from L2/3 of the V1 and retrosplenial cortex, while a full-field grating flash was presented to the contralateral eye of an awake mouse. Flashes with shorter durations induced more evident late responses in mouse V1 LFPs.

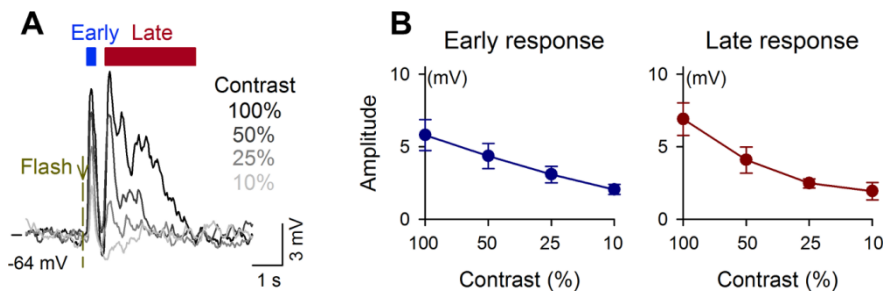


Figure 8. Contrast dependence of flash-induced subthreshold V_m responses. (A) Representative V_m traces after flash stimulation of gratings with contrasts of 100%, 50%, 25%, or 10%. Whole-cell recordings were acquired from V1 L2/3 neurons in awake mice, whose contralateral eyes were presented with 0.05-s grating flashes. (B) Mean \pm SEM of the amplitudes of early and late V_m responses as a function of grating contrast. ($n = 7$ cells from 7 mice).

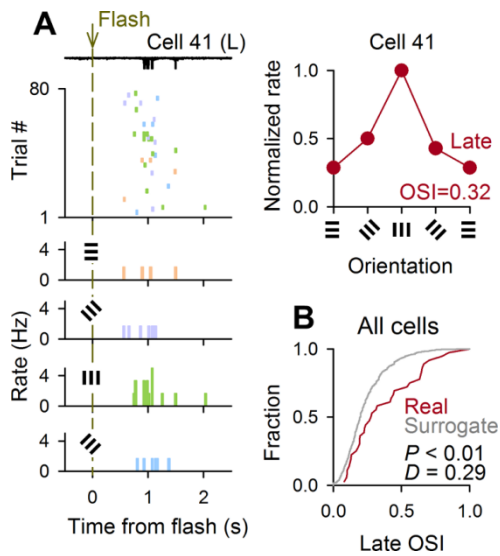


Figure 9. Orientation selectivity of late V1 spike response. (A) Left, raw traces in 10 trials of cell-attached recordings, raster plots of spike responses in 80 trials, and peri-flash time histograms of the firing rates for four orientations of the grating flash stimulation in a representative neuron. The orientations are shown in different colors. Right, the orientation tuning curve of the same neuron. The evoked spike counts were normalized to the maximum. (B) The cumulative probability distribution of the OSIs of the 36 late-spiking cells (Real) was compared with its chance distribution (Surrogate) that was obtained by 1,000 random shufflings of the stimulus trials. The real OSIs were biased rightward compared with the surrogate OSIs ($P = 3.3 \times 10^{-3}$, $D = 0.29$, Kolmogorov-Smirnov test).

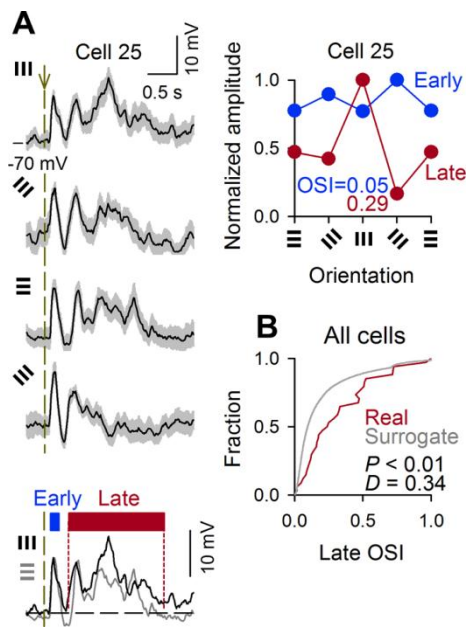


Figure 10. Orientation selectivity of late V1 membrane response. (A) Left traces represent the mean \pm SD of subthreshold V_m responses of an example cell to grating flashes with four orientations. The right plot indicates the orientation tuning curves of the mean amplitude of the early and late V_m depolarizations of the same neuron. (B) The cumulative fraction of the OSIs in the late V_m responses were biased rightward compared with their surrogate OSIs ($n = 34$ neurons, $P = 2.7 \times 10^{-9}$, $D = 0.66$, Kolmogorov-Smirnov test).

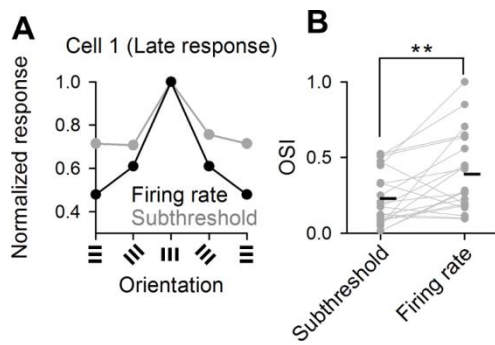


Figure 11. Orientation selectivity of spike responses shows higher tuning than subthreshold responses. Responses to 0.05-s full-field grating flashes were recorded from V1 L2/3 neurons by patch-clamp technique. (A) The representative spike and V_m responses a V1 L2/3 neuron (Cell 1), and its orientation tuning curves of the firing rate (black) and subthreshold V_m responses (gray) are plotted. (B) Mean (black line) and each (gray circle) OSI of the subthreshold V_m responses and firing rates. The OSIs of the spike responses were significantly higher compared with the subthreshold V_m responses ($P = 0.005$, $t_{19} = 3.17$, $n = 20$ cells, paired t -test).

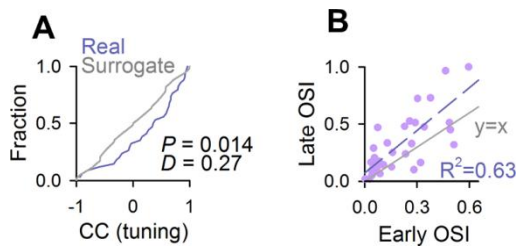


Figure 12. The relationship between orientation selectivity of early and late responses. (A) The correlation coefficients between the early and late tuning curves for individual cells were higher compared with their chance values calculated by random trial-shuffling of the early responses ($n = 34$ neurons, $P = 0.014$, $D = 0.27$, Kolmogorov-Smirnov test). (B) Scatter plots of the OSIs in early and late responses for individual cells. Each dot indicates a single cell. The gray line is the diagonal, and the dash line is the best linear fit.

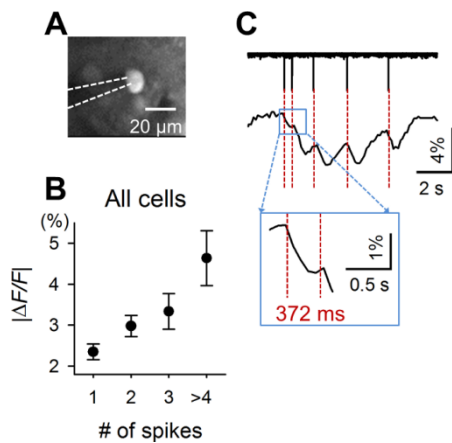


Figure 14. Two-photon calcium imaging visualizes spike responses. (A) Calcium activity from mouse V1 L2/3 neurons was imaged using a two-photon laser microscope. Fura 2 AM, a fluorescence calcium indicator, was locally applied to V1 L2/3. The photograph indicates a two-photon image of a Fura 2-labelled V1 L2/3 neuron. Simultaneous recordings of spikes by cell-attached and calcium imaging techniques were performed on the neuron. The shadow of the patch pipette is outlined by two white dashed lines. (B) The amplitude of the calcium signal ($\Delta F/F$) was plotted against the number of cell-attached-recorded spikes with a time window of 500 ms. Data represent the means \pm SEMs of 5 cells. (C) Individual spikes (top trace recorded in the cell-attached patch-clamp configuration) with the minimal inter-spike-interval of 372 ms could be distinguished by different onsets of calcium transients recorded from the soma. Note that a calcium rise decreases the two-photon fluorescence of Fura 2.

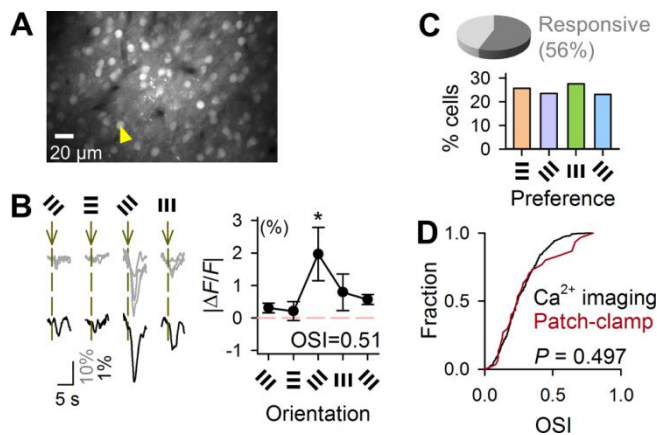


Figure 15. Two-photon calcium imaging of flash-induced V1 responses. (A) The photograph indicates a typical two-photon image of Fura 2-labelled V1 L2/3 neurons. (B) The left traces indicate raw (gray) and mean (black) $\Delta F/F$ of an example cell marked by the arrowhead in (A). The timing and pattern of visual stimuli are indicated above the traces. The right plot indicates the orientation tuning curve of $|\Delta F/F|$ in the same neuron. Error bars represent the SEMs of 12 trials. The baseline is indicated by a pink dotted line. For each stimulus orientation, statistical analyses ($*P < 0.05$ vs baseline, $n = 10-18$ trials, paired t -test) were conducted to determine whether the $|\Delta F/F|$ amplitude was significantly higher than the baseline $|\Delta F/F|$ fluctuations. (C) The top pie chart shows the distribution of cells classified into cells that showed significant $|\Delta F/F|$ responses for at least one orientation (responsive) and cells that showed no activity changes. The bottom bar graph shows the distribution of responsive cells across preferred orientations. (D) The cumulative probability distribution of the $|\Delta F/F|$ OSIs of the 323 responsive cells compared with the late-spiking OSIs of the 31 cells in patch-clamp recordings ($P = 0.497$, Kolmogorov-Smirnov test).

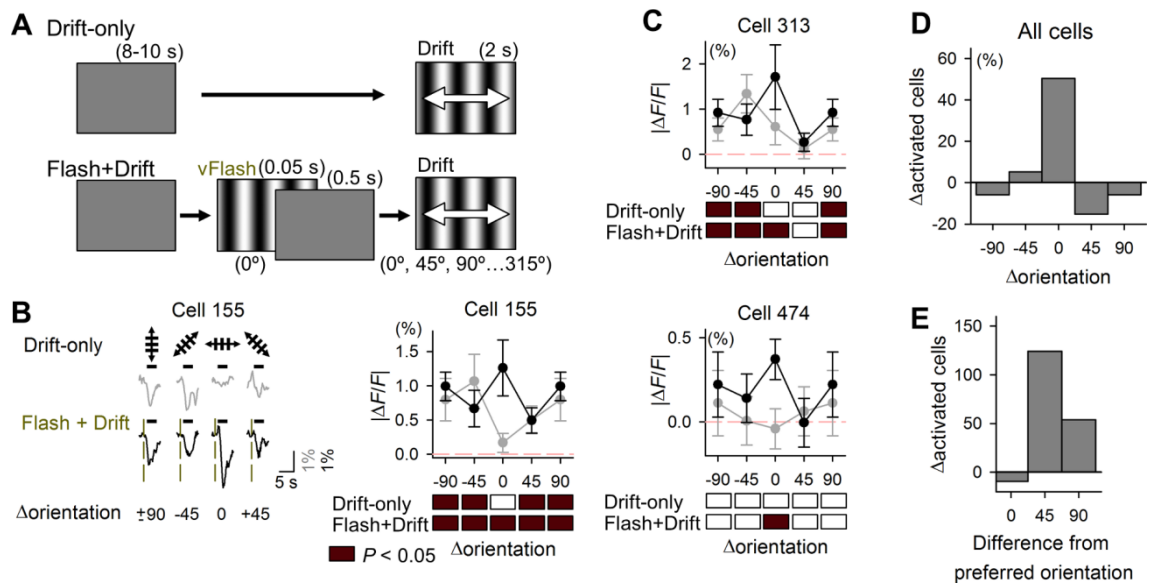


Figure 16. Flash-enhanced V1 response to an identical orientation: multineuron calcium imaging. (A) A schematic shows the visual stimulation protocol without (Drift-only, control) and with (Flash+Drift) 0.05-s full-field grating flashes followed by 2-s drifting-grating stimulus (Drift) presented 0.5 s after vertically grating flashes (0° , vFlash). Drift-only and Flash+Drift trials were applied in a random order, and the responses were compared to measure how the preceding vFlash modulated the $\Delta F/F$ response to Drift with eight directions. (B) Neuronal responses to visual stimuli were recorded using two-photon calcium imaging. The left panel indicates raw $\Delta F/F$ traces at Drift-only trials (gray) and Flash+Drift trials (black) in cell #155. The timing and pattern of visual stimulation are indicated above the traces. The stimulus combination was described as Δ orientation, which indicates the orientation difference between the Drift and vFlash. The right plot is the orientation tuning curve of the mean $|\Delta F/F|$ in the same neuron. Error bars represent the SEMs of 14 trials. Drift-only and Flash+Drift trials are shown in gray and black, respectively. The baseline is indicated by the pink dashed line. For each stimulus orientation, statistical analyses ($*P < 0.05$ vs baseline, $n = 10-18$ trials, paired t -test) were conducted to determine whether the $|\Delta F/F|$ amplitude was significantly

higher compared with the baseline $\Delta F/F$ fluctuation. Dark red boxes below the tuning plot indicate significant responses, whereas open boxes indicate non-significant responses. (C) Three other examples of the $|\Delta F/F|$ orientation tuning curves and the statistical results. (D) Data are summarized from 581 cells. For each Δ orientation, the numbers of cells that exhibited significant $|\Delta F/F|$ responses between Drift-only and Flash+Drift trials were compared ($n = 581$ cells from 11 mice). More cells became responsive at Δ orientation = 0° . (E) The data analyzed in (D) was resolved based on the orientation preferences of individual neurons.

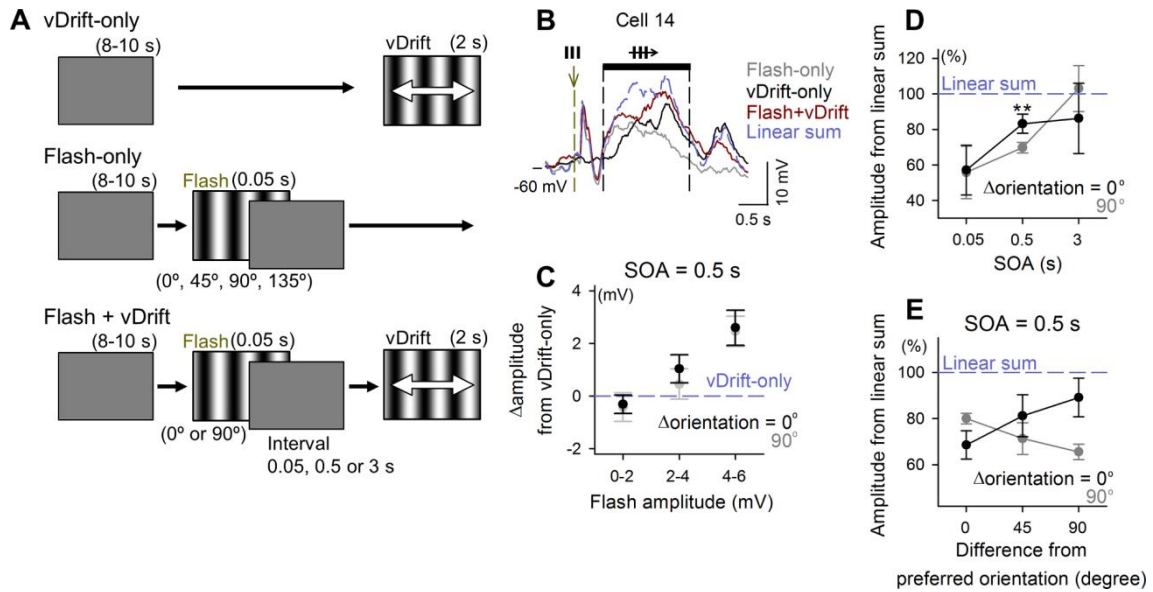


Figure 17. Flash-induced facilitation of V_m response to subsequent visual information. (A) A schematic showing the visual stimulation protocol without (vDrift-only, control) and with (Flash+vDrift) 0.05-s full-field grating flashes followed by 2-s drifting vertical gratings (vDrift) with various stimulus-onset asynchronies (SOA). vDrift-only and Flash+vDrift trials were compared to measure how the preceding flash modulated the V_m response to vDrift. In some of the trials, Flash was presented alone (Flash-only) to record flash-induced responses. (B) Mean subthreshold V_m responses of a representative whole-cell recorded neuron (S4_Data). The timing and pattern of visual stimulation are indicated above the traces. The linear sum of responses was calculated by a simple addition of Flash-only and vDrift-only responses. (C) Means \pm SEMs of the amplitudes of the Flash+vDrift responses relative to vDrift-only responses at a SOA of 0.5 s were plotted against the amplitudes of the Flash-only responses. The stimulus combination was described as Δ orientation, which indicates the orientation difference between the Drift and vFlash. Black and gray symbols indicate Δ orientation = 0° and 90° , respectively. (D) Means \pm SEM of the amplitude of the Flash+vDrift response relative to

the linear sum at SOA of 0.05, 0.5, and 3 s. Black and gray symbols indicate Δ orientation = 0° and 90° , respectively (0.5 s: $**P = 5.0 \times 10^{-3}$ versus Δ orientation = 90° , $t_{25} = 3.07$, $n = 26$ cells from 25 mice, paired t -test). (E) The data at an SOA of 0.5 s in (D) were divided along the orientation preferences of the neurons.

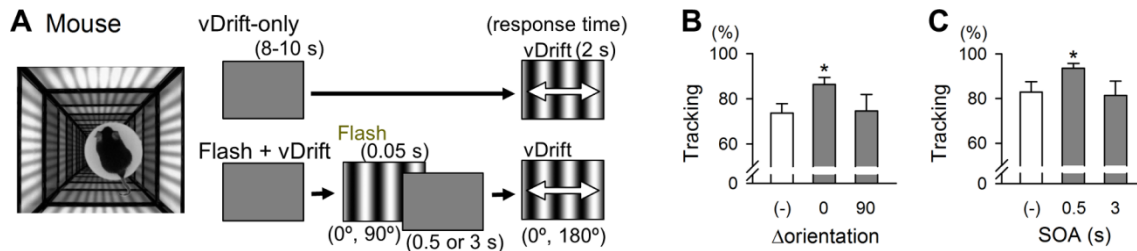


Figure 18. Flash-enhanced visual perception in mice. The visual perception of mice was examined using visual detection tasks. (A) The left photograph shows the virtual optomotor system in which a mouse was placed on the platform surrounded by four computer screens. When vertical gratings that drifted rightward or leftward (vDrift) were presented for 2 s on the computer displays, the mouse may have reflexively moved its head toward the direction of the motion. The ratio of trials that exhibited this tracking response to all trials was used as a measure of visual detection ability. The right schematics show the visual stimulation protocol without (vDrift-only, control(-)) and with (Flash+vDrift) 0.05-s full-field grating flashes presented 0.5 or 3 s before vDrift. Vertical and horizontal grating flashes were used as Δ orientation = 0° and 90° , respectively. (B) Tracking rates of vDrift-only and Flash+vDrift trials at a delay time of 0.5 s. The tracking rates significantly increased at Δ orientation = 0° (* P = 0.037, t_9 = 2.45, n = 10 mice, paired t -test). (C) The flash increased the tracking rates only when vDrift was presented with a delay time of 0.5 s, which was comparable to the timing of the Flash-induced late responses (* P = 0.020, t_{10} = 2.76, n = 11 mice, paired t -test).

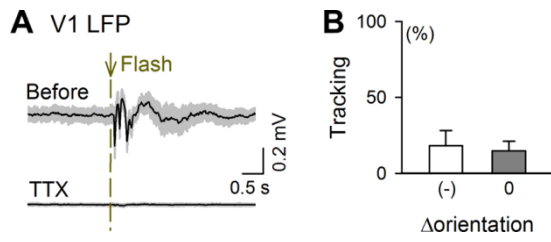


Figure 19. Effect of local application of tetrodotoxin to V1 on mouse head-tracking responses. (A) Mean \pm SD of local field potentials (LFPs) were recorded from V1 before (top) and 10 min after (bottom) local application of tetrodotoxin (TTX, 10 μ M) to the V1 surface. Tetrodotoxin blocked flash-induced LFP responses. This effect lasted more than 120 min after the TTX application. (B) The tracking rates in vDrift-only (-) and Δ orientation = 0 $^\circ$ trials were measured 50-95 min after the TTX application ($n = 4$ mice).

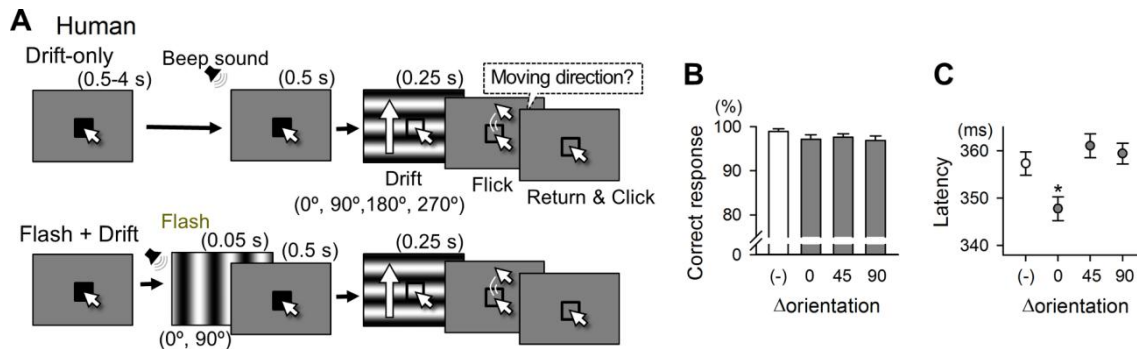


Figure 20. Flash-enhanced visual perception in humans. The visual perception of humans was examined using visual detection tasks. (A) Schematic of the behavioral procedure of a visual motion detection task in humans. In each trial, a Drift was presented in one of four motion directions to which the subject was required to respond by flicking a computer mouse. In Flash+Drift trials, flashes were presented with beep sound cues, whereas in Drift-only trials, the sound cues were applied at the same timing without flash stimuli. (B) The percentage of correct responses to all relevant trials was comparable between the stimulus conditions. (C) The response latency from the Drift stimulus onset was significantly shorter for the $\Delta\text{orientation} = 0^\circ$ ($*P = 0.007$, $t_{993} = 2.71$, $n = 497\text{-}498$ trials from 11 humans, Student's t -test). Error bars represent the SEMs.

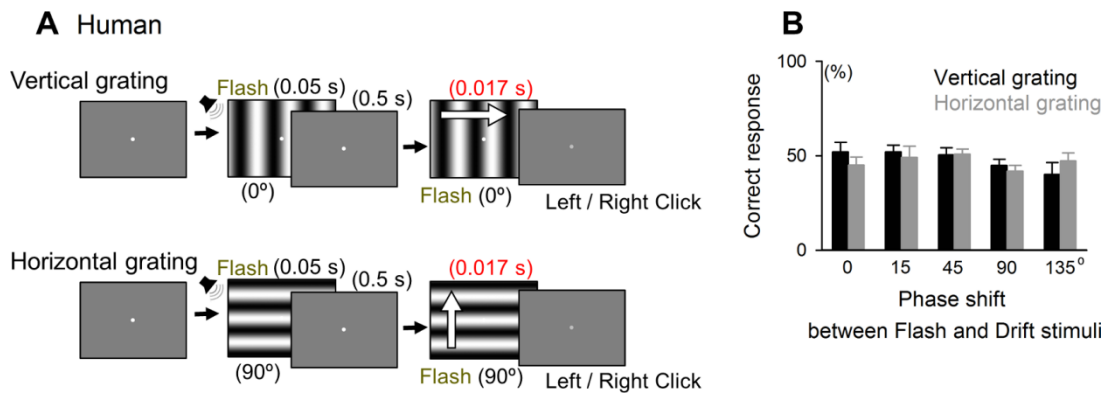


Figure 21. Effect of phase differences between two flashes on motion perception.

(A) Schematic of the behavioral procedure of a visual motion detection task in humans. In each trial, either vertical or horizontal flash was presented 0.5 s before in one video frame of another flash (0.017 s) to which the participants were required to respond "the motion direction" by pressing a left or right arrow-key. The phase of the grating for two flashed was randomized to examine whether the phase shift would induce a motion perception. (B) The correct response rate of the participants did not differ from the chance level, *i.e.*, 50% ($P = 0.254$, $F_{4,40} = 1.39$, $n = 5$ participants, two-way ANOVA), which indicates that the phase shift between two flashes did not induce motion illusion.

Chapter 2

Origin of Neocortical Rebound Depolarization

ABSTRACT

The primary visual cortex exhibits a late response as well as an immediately early response to a visual stimulus. This late response may associate with various visual functions such as sensory perception, iconic memory, working memory, and admixture of timely separated stimuli. However, despite many studies on its functional role, how the late response is organized in the neuronal network is surprisingly unclear. Here, we challenged this question by utilizing a long-delayed response of the primary visual cortex of mouse to a brief flash visual stimulus. Using in vivo whole-cell patch clamp recordings, we monitored synaptic inputs to a neuron during a flash stimulus. We revealed that the late response was constructed by a balanced increase in excitatory and inhibitory conductances and were accompanied by occasional action potentials. The timing of action potentials was predominantly determined by intermittent inhibitory barrages. By using pharmacological and optogenetical approaches, we discovered that these late synaptic inputs were produced in the upstream of classical visual feedforward pathway, thereby enabling a functional output of the cortical late response.

INTRODUCTION

The primary visual cortex (V1) is known to be the neocortical entrance for visual information, which reaches V1 via retina and dorsal lateral geniculate nucleus (dLGN) of the thalamus, classically known as a feedforward pathway [1,2]. Through this route, V1 neurons respond with a short latency upon a presentation of a visual stimulus, from hereout we call it an early response. Vast amount of studies mainly targeted this immediate early response, and basic properties of the visual responses are now well-described [41-43, 50, 52, 89]. However, recently, the later part of the visual response is under the spotlight in which it is often associated with sensory perception [90], iconic memory [10,11], and working memory [12-14]. In addition to these findings, we discovered a new response pattern of V1 neurons; Through the use of a brief short visual stimulus (flash), V1 neurons exhibited a long late response as well as the well-known early response [91]. We revealed that this late response may mediate the admixture of two timely-separated visual information, contributing to visual processing. Although we suggested its functional role, it is still unclear how the cortical late response is organized in the neuronal network.

In this study, we first approached a neuronal circuit mechanism of the late response. We patch-clamped V1 layer 2/3 neurons *in vivo* and recorded their synaptic inputs to a brief flash stimulus. We found that both excitatory and inhibitory inputs contribute to the late spike responses, whereas inhibition exerted more control over spike timing. By utilizing pharmacological and optogenetical manipulation of neuronal activity *in vivo*, we revealed that the cortical late response arrives via the identical pathway with the early response. Thus, visual information repetitively travels the same feedforward pathway, achieving the finely shaped organization of the late response.

MATERIALS AND METHODS

Ethical approval

The same as Chapter 1 of this doctoral thesis.

Animal preparation for recordings

The same as Chapter 1 of this doctoral thesis except for that recordings were made under anesthetized state induced by urethane (1.0–1.5g/kg).

Visual stimulation

Visual stimuli were generated in custom-written MATLAB routines (The MathWorks, Natick, MA, USA) with Psychtoolbox extensions. A 17-inch TN-LCD monitor (refresh rate = 60 Hz) was placed 30 cm away from the right cornea, so that it covered 38.8° horizontally and 29.6° vertically of the mouse visual field. For flash stimulation, a white screen (contrast: 100%) was presented, and its duration was set at 50 ms. Flash stimuli were intervened with a gray screen for intervals of 8–10 s, and were repeated for 40-50 times. A gray screen was shown during the interval period.

Electrophysiology

The same as Chapter 1 of this doctoral thesis except for voltage-clamp recordings. The intra-pipette solution consisted of the following (in mM): 130 CsMeSO₄, 4 tetraethylammonium-Cl, 10 HEPES, 10 Na₂-phosphocreatine, 0.5 EGTA, 4 MgATP, 0.3 Na₂GTP, and 2 QX-314.

Dynamic-clamp recording

Current-clamped neurons were stimulated with the dynamic-clamp conductance injection technique [92]. The command current $I(t)$ was calculated online as

$G_e(t) \times (V(t) - E_{e_rev}) + G_i(t) \times (V(t) - E_{i_rev})$, where $G_e(t)$ and $G_i(t)$ were time-varying conductances obtained from voltage-clamp recording; $V(t)$ was the membrane potential at time t ; and the reversal potentials E_{e_rev} and E_{i_rev} were 0 mV for excitation and -90 mV for inhibition. $I(t)$ was delivered into patch-clamped neurons at 20 kHz using a PCI-6024E data acquisition board (National Instruments, Austin, TX) under a real-time Linux environment. The gain of injecting conductance was controlled to induce spikes from patch-clamped neurons.

Wavelet transform of LFP response

We measured the time-varying oscillatory power of the LFP responses using a complex Morlet wavelet (center frequency of 1.5 Hz, bandwidth parameter of 1) defined as:

$$\tilde{x}(t) = \int_{-\infty}^{+\infty} x(t) \varphi_{a,b}(t) dt \quad (\text{Continuous wavelet transform})$$

$$\varphi_{a,b}(t) = \frac{1}{\sqrt{a}} \varphi\left(\frac{t-b}{a}\right)$$

The mother wavelet is defined as:

$$\varphi(x) = \sqrt{\pi f_b} e^{2i\pi f_c x} e^{-\frac{x^2}{f_b}} \quad (\text{Complex Morlet wavelet})$$

a: scale factor

b: shift (1/sample rate)

f_c : center frequency

f_b : bandwidth parameter

Scale factor (a) was set at frequencies between 1-60 Hz with interval of 1 Hz.

Mouse lines

Vgat-Cre mouse (Jackson Labs stock number: 016962) for Figures 28 and 29.

Virus

AAV5-CaMKII α -hChR2(H134R)-EYFP,

AAV2-EF1 α -DIO-hChR2(H134R)-EYFP

from University of North Carolina vector core.

Virus injection

For Figure 25, 0.5 μ L of AAV2-EF1 α -DIO-hChR2(H134R)-EYFP was injected unilaterally to V1 of wild type C57BL/6j mice. For Figures 28-29, 0.5 μ L of AAV5-CaMKII α -hChR2(H134R)-EYFP was injected unilaterally to thalamic reticular nucleus (TRN) of Vgat-Cre mice. Mice were anesthetized with pentobarbital (0.8 mg/kg) and xylzine (0.8 mg/kg). The head skin was then removed and the small craniotomy was made over either the primary visual cortex (V1, 3.0 mm posterior to the bregma and 2.8 mm ventrolateral to the sagittal suture) or the thalamic reticular nucleus (TRN, 1.5 mm posterior to the bregma and 2.1 mm ventrolateral to the sagittal suture). The virus was pressure-injected at the depth of 1.2 mm (V1) or 3.5 mm (TRN) at the speed of 250 nL/min (Muromachi). The injection pipette was removed 5 min after the injection ended. Recordings were made 4-5 weeks after virus injection.

Optogenetic stimulation

The optic fiber attached to the blue light laser (473 nm, COME2-LB473/100s, Lucir) was illuminated at the target brain region with the power of 10-15 mW. For Figure 25, the blue light was given briefly for 0.05 s, and for Figure 28-29, it was given

continuously for the given time period.

RESULTS

V1 late synaptic inputs

From our previous paper [91], the magnitude of the late response is known to correlate with the stimulus intensity, meaning that the V1 late response involves neuronal circuits of the visual-related regions. From this knowledge, we first focused on the synaptic inputs that shaped the depolarization of the V1 late response. We obtained whole-cell voltage-clamp recordings using a cesium-based internal solution. Individual trial traces and averaged traces of EPSC-dominant and IPSC-dominant currents are shown in Figures 22A and B. The averaged EPSC trace showed a seemingly outward transient current after the early flash response. This was caused, in part, by unperfected voltage-clamping due to the space-clamp problem, as well as by a reduction in tonic excitation that was present under pre-stimulus basal conditions.

We first focused on the background synaptic conductances prior to the presentation of flash stimulus. Individual traces indicated that IPSCs often showed large, barrage-like synaptic inputs compared with EPSCs (Fig. 22A). To quantify this difference in input patterns, we calculated the standard deviation (SD) of membrane potential fluctuations in pre-flash synaptic inputs. Consistent with the eye inspection, G_i indeed had a larger SD than did G_e (Fig. 22C, $**P = 9.79 \times 10^{-13}$, $t_{149} = 7.80$, G_e versus G_i , $n = 150$ trials from 7 cells from 7 mice, Student's t -test). The amplitudes of individual IPSC barrages ranged from roughly 100 to 300 pA and were larger than the unitary IPSCs evoked by single GABAergic synapses [93-94], suggesting that they were produced by synchronized inhibitory inputs from presynaptic interneuron ensembles.

We next analyzed changes in G_e and G_i (ΔG_e and ΔG_i , respectively) during the late responses that were observed 0.4–2.0 s after flash. Since membrane potential might

be imperfectly clamped, we calculated the change in conductance, rather than the absolute values, by subtracting the pre-stimulus mean value. This calculation is also expected to cancel out the possible effect of cesium-based solution; note that caesium ion may block ion channels associated with the resting conditions. The time-evolution plot of the mean ΔG_e and ΔG_i across all 7 cells shows that ΔG_e was nearly proportional to ΔG_i for the entire period of 1.6 s (Fig. 22D), indicating that excitatory and inhibitory inputs are co-tuned at a given time point. For individual trials, however, the pattern of flash-induced conductance changes was different between G_e and G_i . That is, the G_e increases seemed to be shaped by a tonic increase in synaptic inputs, whereas the G_i increases seemed to arise from an increase in the number of large IPSC barrages (Fig. 22A). Indeed, the mean G_e and G_i values increased to similar degrees in response to flashes (Fig. 22E), whereas an increase in SD was observed in G_i , but not in G_e (Fig. 22F, $**P = 2.91 \times 10^{-19}$, $t_{149} = 10.35$, G_e versus G_i , $n = 150$ trials from 7 cells from 7 mice, Student's t -test).

Inhibitory barrages determine spike timing

Even though the overall balance of excitatory and inhibitory synaptic inputs was maintained during late response, the input patterns differ for individual trials. This implicates that excitatory and inhibitory inputs could be transiently imbalanced and thereby contribute to late spike timings. To determine the synaptic mechanisms for emitting late spikes, it is important to examine which of the two synaptic inputs exerted more control over spike timings. We sought to reveal this issue using the dynamic-clamp conductance injection technique. After dendrogram clustering (Fig. 23), we selected four discrete patterns of G_e and G_i obtained from the voltage-clamp

recordings (2.5-s periods after flashes) and subtracted the pre-flash baseline from these values (ΔG_e and ΔG_i , respectively). We injected arbitrary combinations of single ΔG_e and ΔG_i traces into current-clamped neurons (Fig. 24A) and found that the neurons spiked at times when ΔG_i became small (Fig. 24B, C). Spike-triggered averages of injected conductances revealed that ΔG_i exhibited a larger change (time-locked to a spike) than did ΔG_e (Fig. 24D). These data suggest that although both excitatory and inhibitory inputs contributed to spikes, they were involved in different ways; tonic increases in ΔG_e depolarize the membrane potential, whereas intermittent drops in ΔG_i provide opportunities for evoking spikes. Consistent with previous reports [95-96], these results indicate that inhibitory inputs have greater effects on spike timing than do excitatory inputs.

Late response flows through the feedforward pathway

From the above investigations, we found that the late response was constructed by synaptic inputs, meaning that it arises in network level. Thus, we next sought for the brain region in which the late response was generated. We examined three major candidates: (1) Recurrent projection, in which the late response is generated and amplified through V1 networks [98], (2) feedback projection from higher-order cortices [59, 97], in which the late response is dependent on the top-down inputs, (3) feedforward projection, in which the late response is generated in the upstream of V1 and travels the bottom-up pathway.

We first examined whether direct activation of V1 network, mimicking the flash-induced early response, induces late response; in other words, we tested if transient activation of V1 without prior dLGN or retinal activity is sufficient to generate

a late rebound activity. We employed an optogenetic approach by expressing channelrhodopsin 2 (ChR2) into V1 through virus injection (AAV5-CaMKII α -hCHR2(H134R)-EYFP). 4-5 weeks after viral injection, robust ChR2 expression was observed within the visual cortex (Fig. 25A). By brief illumination of blue light, direct and transient activation of V1 was achieved. On the recording session, we alternately presented flash (flash stimulus) and blue light (ChR2 stimulus) and monitored LFP responses from V1 (Fig. 25B). As a result, flash stimulus distinctively induced strong late LFP powers whereas ChR2 stimulus failed to induce the persistent late activity (Fig. 25C). ChR2 stimulation-induced LFP powers during the late response (>0.4 s, <2.0 s) showed significantly lower magnitude than flash-induced late response (Fig. 25D and 25E, * P = 0.032, t_5 = 2.95 (4-12 Hz); * P = 0.025, t_5 = 3.15 (14-30 Hz); * P = 0.019, t_5 = 3.41 (30-60 Hz); n = 6 mice, paired t -test). Thus, V1 recurrent network is unlikely to be the initiation site of the V1 late response.

Next, we tested whether V1 late response was dependent on the activity of higher-order cortices. From previous studies using voltage sensitive dyes in mice, visual information flows from V1 to anterior cingulate cortex (ACC) as well as to the secondary visual cortex (V2) [33, 97]. These higher cortical regions project back and modulate the activity of the primary sensory cortices [97]. Thus, we tested if inhibition of ACC demolishes the V1 late response. We applied tetrodotoxin (10 μ M), the voltage sensitive sodium channel inhibitor, to the surface of ACC and waited for 20 min, which drastically inhibited its neuronal activity. Then, we recorded flash-evoked LFP responses in V1 (Fig. 26A). Consistent with the previous reports, application of tetrodotoxin significantly reduced the flash-induced late LFP powers (Fig. 26B and 26C, ** P = 0.0035, t_5 = 5.19 (4-12 Hz); * P = 0.014, t_5 = 3.68 (14-30 Hz); * P = 0.039, t_5 =

2.77 (30-60 Hz); $n = 6$ mice, paired t -test). However, its effect was small, where much of the late response was left intact. Thus, although the feedback projection from ACC partially modulates the V1 late response, it is unlikely to be the major synaptic driver.

Lastly, we examined the possibility that the late response takes the same path as the early response. In other words, the V1 late response might be generated in the upstream of the visual pathway. We recorded multi-unit recordings from dorsal lateral geniculate nucleus (dLGN), and presented the flash stimulus. To make access to dLGN more convenient, parts of the primary somatosensory cortex and the hippocampus above dLGN were removed (Fig. 27A). With this treatment, even in vivo patch-clamp recordings became routinely possible to monitor the single cell dynamics of individual dLGN neurons (Fig. 27B). Similar to V1, flash stimulus induced both early spikings and late spikings in dLGN (Fig. 27C and 27D). Using tetrodotoxin, we confirmed that this dLGN response was not inhibited by V1 inactivation, denying the possibility that the thalamo-cortical-loop producing the late response (Fig. 27E).

Although a flash evoked late response in dLGN, V1 might be receiving late synaptic inputs via other alternative pathways [1, 99]. To confirm the necessity of dLGN activity on V1 late response, we examined whether inhibition of dLGN suppresses the late response observed in V1. If this hypothesis is true, it means that the late response takes the same pathway as the early response; thus, dLGN should be silenced specifically at the timing of the late response, leaving the early response intact. We again utilized the optogenetic approach. We consulted the technique that Massimo Scanziani's group took [100]. To shut down the relay neurons of the dLGN, we expressed ChR2 to thalamic reticular nucleus (TRN) [101], which sends direct GABAergic projection to dLGN [102-103]. We conditionally expressed ChR2 on Cre

recombinase by injecting Cre-dependent adeno-associated virus encoding ChR2 into TRN of the Vgat-Cre transgenic mouse (Fig. 28A and B, expresses Cre in GABAergic neurons, 104). By illuminating ChR2 expressing GABAergic axons in dLGN immediately after the flash-evoked early response (>0.2 s), we powerfully suppressed dLGN activity with high temporal-resolution (Fig. 28C, reducing $70.4 \pm 11.7\%$ of its spikes (Fig. 28D, $*P = 0.0162$, $t_2 = 7.76$, $n = 3$ recordings from one mouse, paired- t -test). Using this technique, we monitored V1 LFP responses to the flash stimulus (Fig. 29A). The specific silencing of dLGN at the time of the late response rapidly and selectively suppressed the V1 late response whereas the early response was intact. LFP power at each frequency band was dramatically reduced (Fig. 29B and 29C, $*P = 0.036$, $t_3 = 3.63$ (4-12 Hz); $*P = 0.015$, $t_3 = 5.05$ (14-30 Hz); $n = 4$ mice, paired t -test). Therefore, V1 late response is deeply depended on the synaptic inputs from dLGN.

DISCUSSION

In this study, we revealed the organization of synaptic inputs that constitute the V1 late response. We discovered that the late response was produced by a balanced increase in G_e and G_i , while the dynamics of G_i were more powerfully influential in controlling the spike timing of the neuron. These synaptic inputs were recruited via the thalamo-cortical activity of dLGN, meaning that the late response travels through the same feedforward pathway as the well-known early response.

Since we observed robust excitatory and inhibitory inputs during the flash-evoked late response in V1, the cortical late response is most likely shaped up by synaptic inputs and not by the cell-autonomous rebound activity. In accordance with this, we were able to reproduce the late response in any L2/3 neurons of V1 when we gave late synaptic conductance through the dynamic clamp technique (Fig. 24). However, a transient activation of V1 recurrent network failed to produce the late response. Therefore, it is suggested that the initiation site of the late response lies in a different brain region besides V1.

From various studies, the top-down control from higher-order cortices often modulates the later part of the sensory response [59, 97]. This feedback activity is often related to sensory perception, and in the case of the vision, the anterior cingulate cortex (ACC) is known to modulate the primary visual cortex via this pathway [97]. Although we did not test if the late response that we found contributes to perception, the silencing of ACC significantly reduced the late LFP power of the flash response. However, its effect was only partial, and much portion of the late response remained. Thus, we speculate that a higher-order cortex modulates the V1 through feedback activity, but it may not be the essential driver of the late response.

We observed that a flash stimulus induced both early and late spikings in dLGN. At the same time, selective optogenetic silencing of dLGN, which transmits visual information to V1, clearly abolished the V1 late response which was reduced to the level of the spontaneous activity. This result shows that generation of the cortical late response depends highly on the thalamic activity. However, there was another possibility. The primary sensory thalamus often makes thalamo-cortical loop with the primary sensory cortex in which L6 cortical neurons give direct excitatory projections to the primary sensory thalamus [105]. This cortico-thalamic projection accounts for up to 40% of the synapses made in dLGN whereas retinal inputs take up only about 10% [106]. Thus, this thalamo-cortical loop could be the alternative for the initiation site of the late response. However, we confirmed that V1 inactivation did not disrupt the thalamic late response. Therefore, we conclude that the upstream of the classical feedforward pathway, either dLGN or retina, is the best candidate for the origin of the late response.

Then, does the cortical late response merely reflect the thalamic response? In terms of the sensory response, the majority of the inputs arriving to a cortical neuron derive from the cortical recurrent network [107]. Notably, this sensory activity is abolished when a primary sensory thalamus of that modality is suppressed [100]. Therefore, the cortical recurrent network greatly amplifies the thalamic input, but only with the existence of the thalamic activity. Consistence with this idea, thalamic late response is much smaller compared with the early response whereas cortical late response is comparable with the early response. Thus, we speculate that the late response may exert its function only when it reaches the cortex. Indeed, the effect of the flash stimulus on later coming visual processing depended on the activity of the primary

visual cortex [91].

Although, we found that the late response travels the same route as the classical feedforward pathway, it is still unresolved how this sequential information is processed. Future work is necessary on how timely separated responses of early and late responses are integrated and/or discriminated in the visual perception of an animal.

FIGURES

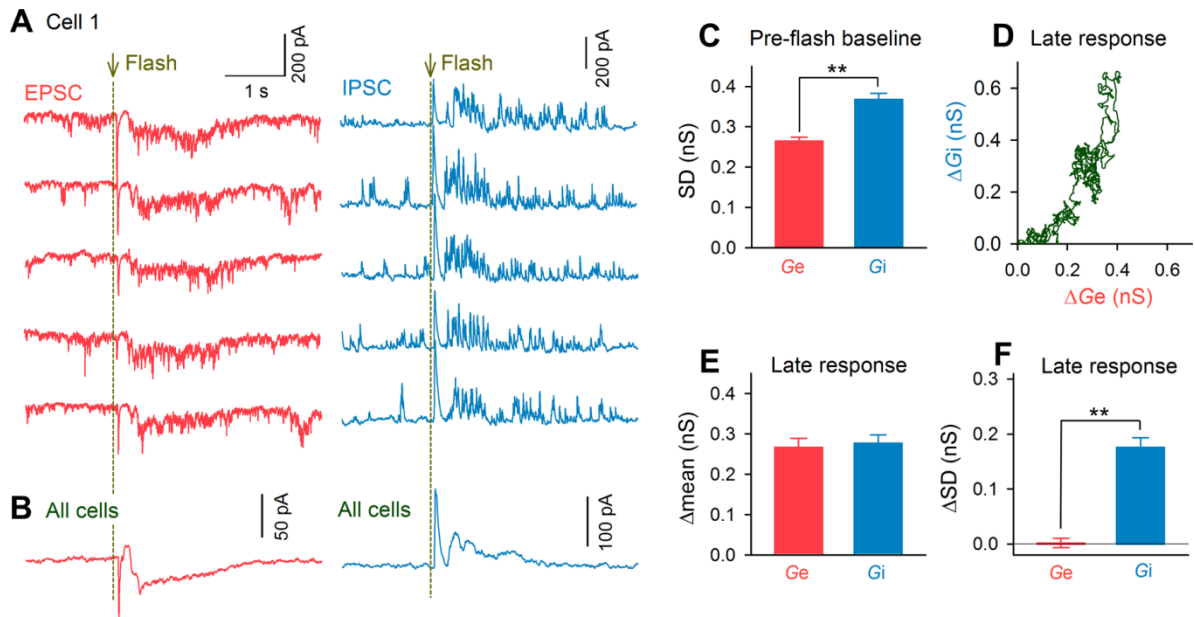


Figure 22. Light flashes differentially modulate excitatory and inhibitory conductances. (A) Whole-cell current-clamp recordings were acquired from layer 2/3 primary visual cortical neurons, and 20-50 trials of flashes were presented to the contralateral eye. EPSCs and IPSCs were recorded at clamped voltages of -74 mV and 0 mV, respectively. Five randomly selected traces of EPSCs and IPSCs from a representative neuron are shown. (B) Mean EPSC and IPSC traces of 7 cells from 6 mice. (C) The mean SDs of G_e and G_i fluctuations during individual trials in the pre-flash baseline period. Error bars indicate SEMs of 230 trials from 7 cells. $**P = 9.79 \times 10^{-13}$, $t_{149} = 7.80$, G_e versus G_i , $n = 7$ cells from 7 mice, Student's t -test. (D) Time course of the relationship between the mean G_e and G_i during late responses. Data are the same as in (B). (E,F) Comparisons of flash-induced changes in the means (E) and SDs (F) of G_e and G_i during the late responses ($**P = 2.91 \times 10^{-19}$, $t_{149} = 10.35$, G_e versus G_i , $n = 150$ trials from 7 cells from 7 mice, Student's t -test).

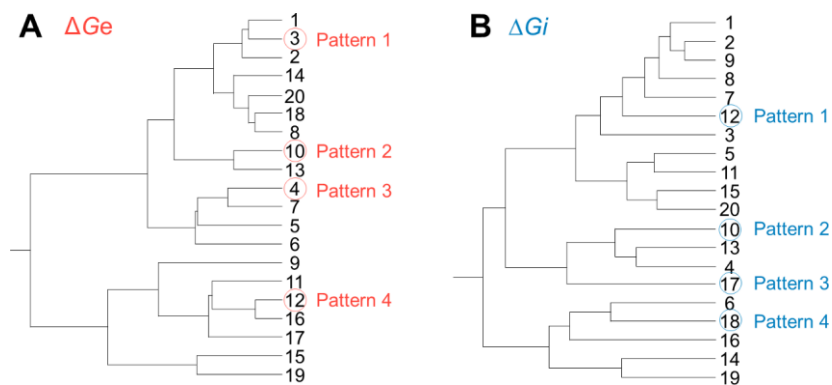


Figure 23. Different synaptic input patterns were used in dynamic clamp experiments in Figure 24. EPSC and IPSC traces were classified by Ward's method, and four traces were selected from each dendrogram to generate synaptic conductance patterns, ΔG_e and ΔG_i .

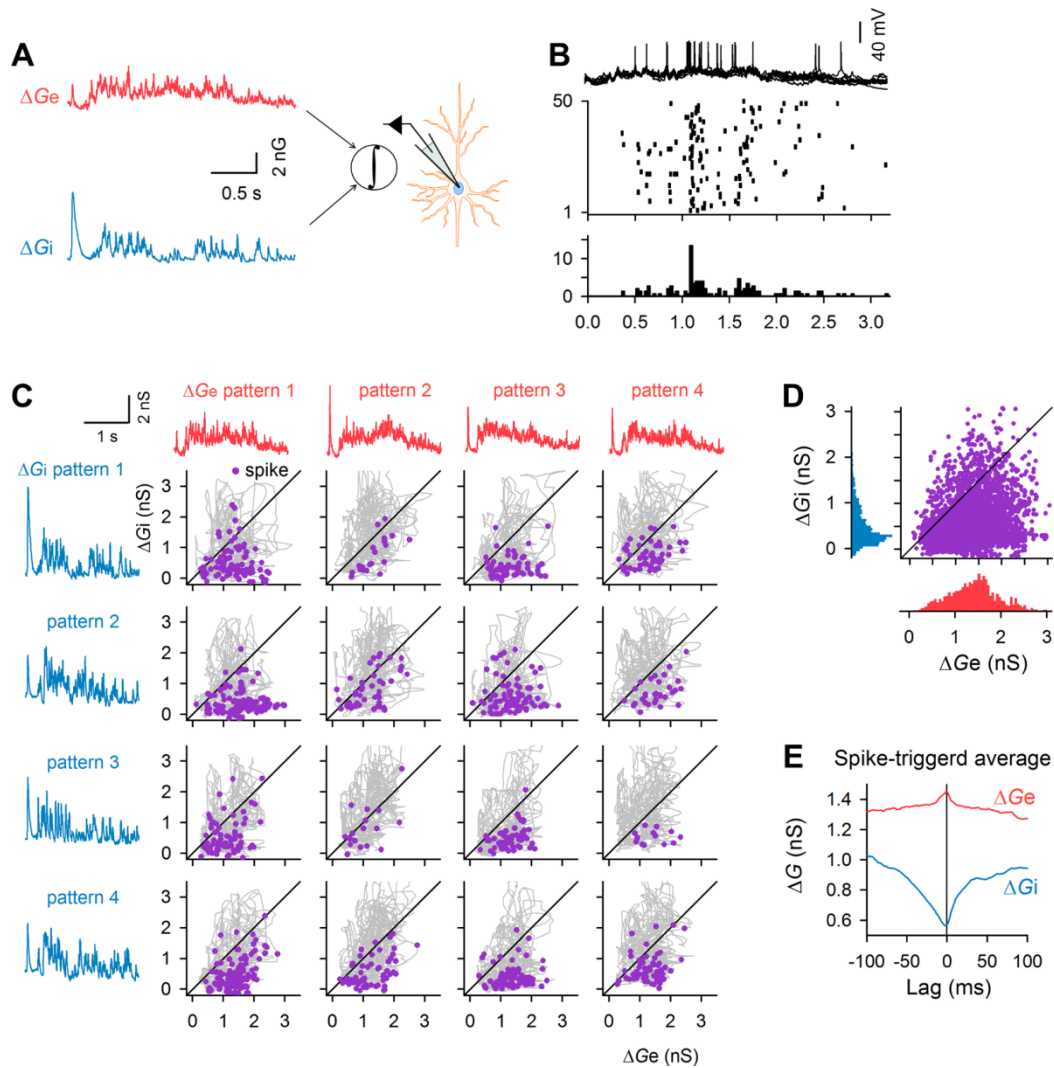


Figure 24. Inhibitory inputs determine the timing of late spikes. (A) Current-clamped neurons were stimulated with the dynamic-clamp technique. Time-varying ΔG_e and ΔG_i after flashes were obtained from voltage-clamp recordings. Four patterns of each ΔG_e and ΔG_i (2.5 s in length) were paired, yielding a total of 16 ($=4 \times 4$) patterns of mixed conductances. (B) Each conductance pattern was injected for 20–50 trials. (Right top), five traces from a representative neuron. (Right bottom), raster plot of evoked spikes from all 50 trials. (C) Relationships between the ΔG_e and ΔG_i levels and spikes recorded from a single representative neuron. Only late spikes during the post-flash period of 0.4–2.0 s were analyzed. Gray lines indicate the trajectories in

the space of ΔG_e and ΔG_i as a function of time. Purple dots indicate the timing of spikes on the trajectories. (D) Summary data for all 6 neurons. The *left* and *bottom* histograms indicate the distributions of spike counts. (E) Spike-triggered average of ΔG_e and ΔG_i for all 4885 spikes.

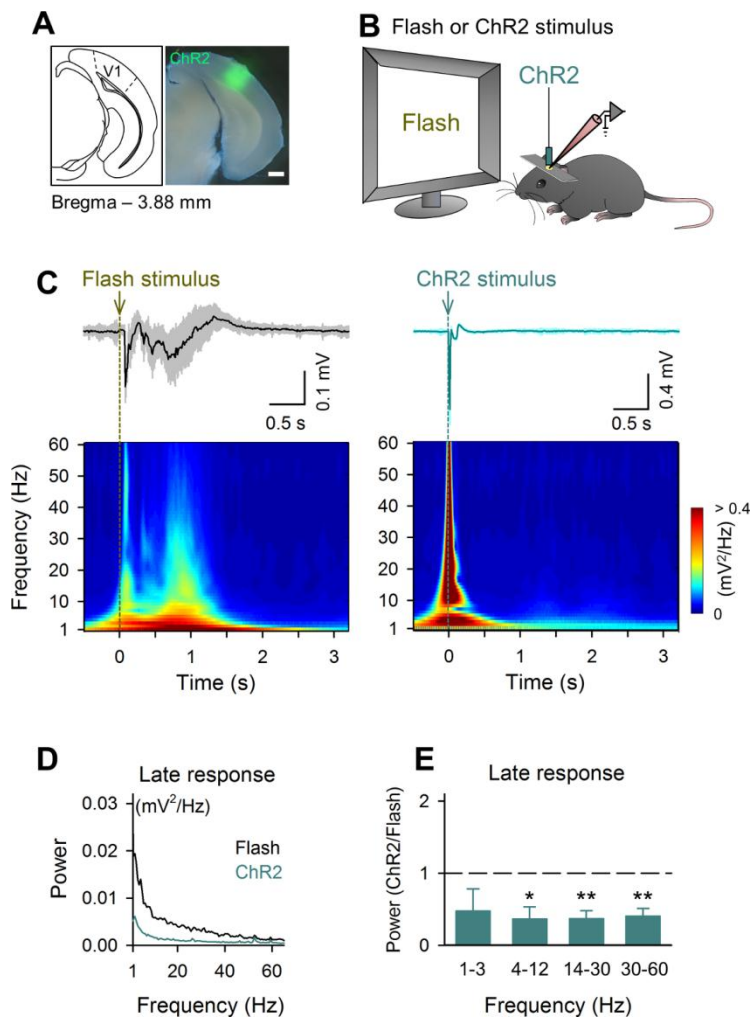


Figure 25. Transient optogenetic activation of V1 does not induce V1 late response.

(A) A schematic of ChR2 expression. AAV5-CaMKII α -hCHR2(H134R)-EYFP was injected to V1 of 7-8 week-mice. Scale bar = 0.5 mm (B) A schematic of an experimental protocol. LFP recordings were acquired from layer 2/3 of the V1. Flash stimulus (visual stimulus) to the contralateral eye and ChR2 stimulus (transient optogenetic stimulation) to ipsilateral V1 were alternately presented to the mouse for 50 trials, respectively. (C) (Top) Mean \pm SD of stimulus-evoked LFP traces. (Bottom) Mean powers of stimulus-evoked LFP for each frequency band using the wavelet transform. The left and right columns show the results for flash stimulus and ChR2 stimulus, respectively. (D) The mean LFP power for each frequency during the time

window of late response (0.4–2.0 s) was analyzed using fast Fourier transform. (E) Comparison of LFP powers for each frequency band between ChR2 and Flash stimulus trials for all animals (* $P = 0.032$ (4-12 Hz), * $P = 0.025$ (14-30 Hz), * $P = 0.019$ (30-60 Hz), $n = 6$ mice, paired t -test).

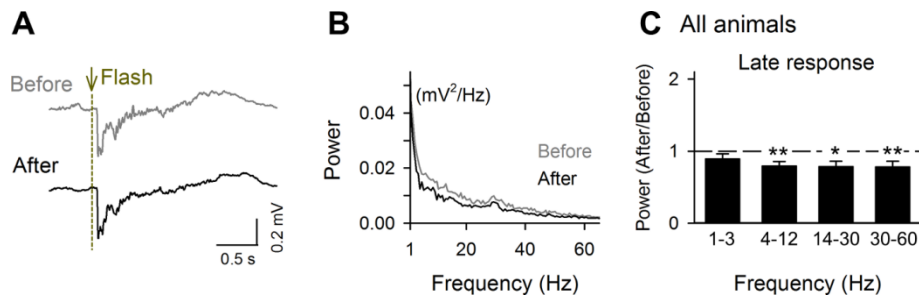


Figure 26. Inhibition of M2/ACC weakly reduces the V1 late response. LFP recordings were acquired from layer 2/3 of the V1, and 50 trials of flashes were presented to the contralateral eye. (A) LFP Recordings were made before (Before) and after (After) the surface application of tetrodotoxin (10 μ M) over M2 and ACC. (B) The mean LFP power for each frequency during the time window of late response (0.4–2.0 s) was analyzed using fast Fourier transform. (C) Comparison of LFP powers for each frequency band between before and after tetrodotoxin application for all animals (** $P = 0.0035$ (4-12 Hz), * $P = 0.014$ (14-30 Hz), * $P = 0.039$ (30-60 Hz), $n = 6$ mice, paired t -test).

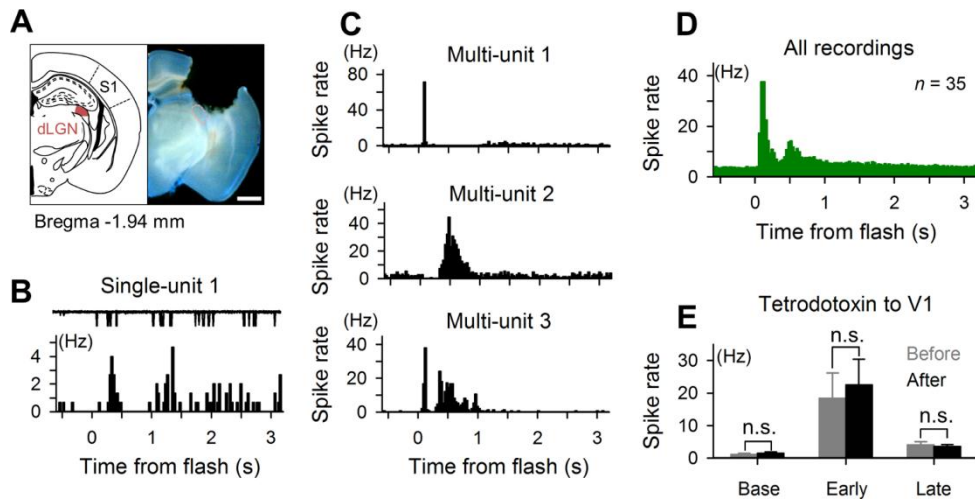


Figure 27. Flash-evoked biphasic spike responses in dorsal lateral geniculate nucleus (dLGN). (A) A part of the primary somatosensory cortex (S1) and hippocampus were acutely removed to expose the dorsal LGN (dLGN). Single (B) and multi-unit recordings (C) were acquired from dLGN, and the flash stimulus was presented to the contralateral eye for 50 trials. (A) An example photo of the coronal slice stained by Hoechst (1:1000). The part of the primary somatosensory cortex and the hippocampus were removed to access dLGN (the red-framed area). Scale bar = 0.5 mm (B) The representative single unit recording of a dLGN neuron, which exhibits robust late response. (Top) Raw spike response trace of 10 representative trials. (Bottom) Peri-stimulus time histogram (PSTH) of the spike response. (C) Three representative examples of PSTHs of spikes from multi-unit recordings. (D) Data from 35 recordings from 19 mice were pooled. (E) Pre-stimulus spike rate (Base), early spike rate (Early, < 0.2 s), and late spike rate (Late, >0.4 s, <2.0 s) of dLGN multi-unit recordings before and after the surface application of tetrodotoxin (10 μ M) to V1 ($P > 0.05$, $n = 6$ mice, paired t -test).

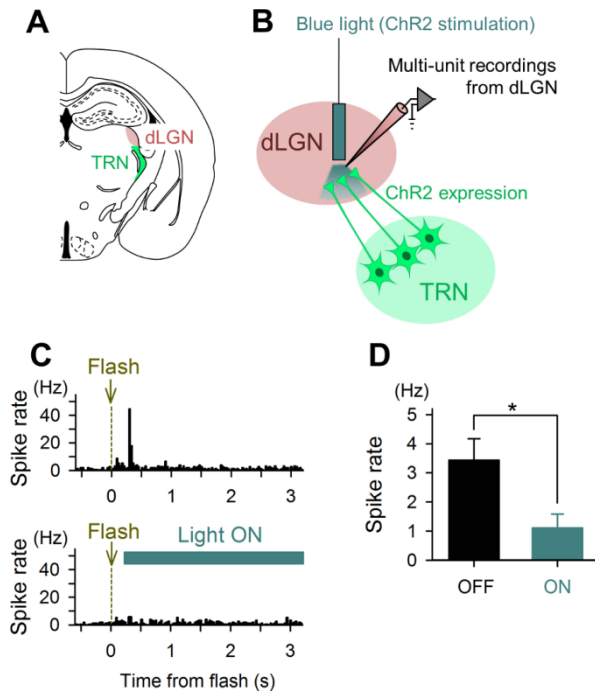


Figure 28. Selective inhibition of dLGN during the time window of V1 late responses. (A) The schematic of the virus injection to the thalamic reticular nucleus (TRN). AAV2-EF1 α -DIO-hChR2(H134R)-EYFP was injected to TRN of Vgat-Cre transgenic mice to selectively induce ChR2 on TRN GABAergic neurons. (B) A schematic of the experimental protocol. Multi-unit recordings were acquired from dLGN. The blue light was given to the dLGN to activate the ChR2 expressing axons of TRN neurons, resulting in the specific inhibition of LGN neurons. (C) Multi-unit recordings were acquired from dLGN, and 50 trials of flashes were presented to the contralateral eye with (light ON) or without (light OFF) blue light stimulation. On light ON trials, the blue light was presented 0.2 s after flash stimulus in order to specifically inhibit dLGN at the time window of late response, leaving the early response intact. (D) Mean \pm SEM multi-unit spike rates of light ON and light OFF trials, respectively ($*P = 0.0162$, $n = 3$ recordings from one mouse, paired t -test).

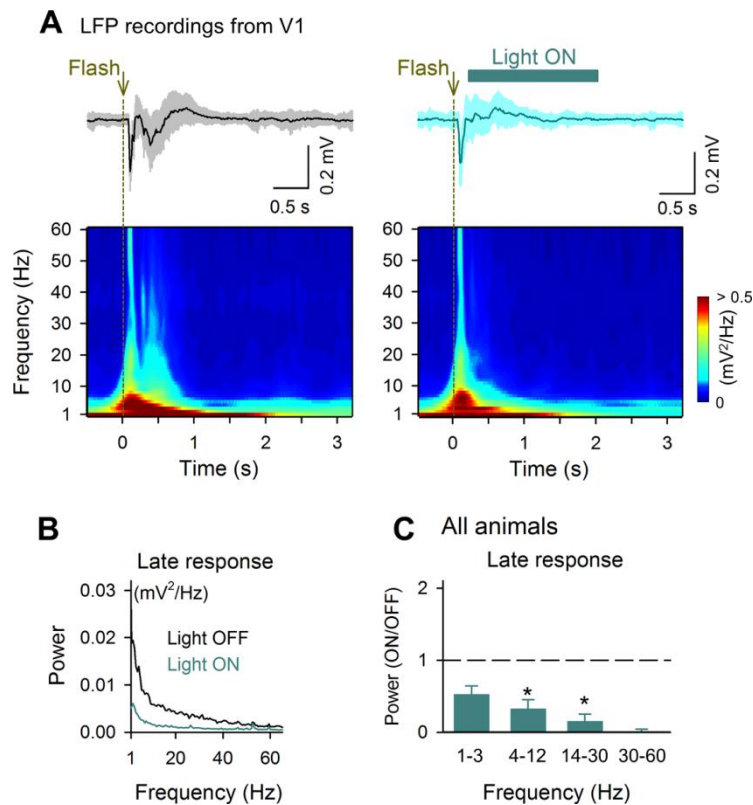


Figure 29. Selective inhibition of dLGN dramatically suppressed the V1 late response. (A) LFP recordings were acquired from layer 2/3 of the V1, and the flash stimulus was presented to contralateral eye. The blue light was given to the dLGN to activate the Chr2 expressing axons of TRN neurons, resulting in the specific inhibition of LGN neurons at the timing of the late response. 50 trials of visual responses were recorded for blue light ON (Light ON) and blue light OFF (Light OFF) trials, respectively. (Top) Mean \pm SD of stimulus-evoked LFP traces. (Bottom) Mean powers of stimulus-evoked LFP for each frequency band using the wavelet transform. The left and right columns show the results for light OFF and light ON trials, respectively. On light ON trials, the blue light was presented 0.2 s after flash stimulus in order to specifically inhibit dLGN at the time window of late response, leaving the early response intact. (B) The mean LFP power for each frequency during the time window of late response (0.4 – 2.0 s) was analyzed using fast Fourier transform. (C) Comparison of

LFP powers for each frequency band between light ON and OFF trials for all animals

(* $P = 0.036$ (4-12 Hz), * $P = 0.015$ (14-30 Hz), $n = 4$ mice, paired t -test).

REFERENCE

1. Felleman DJ, Van Essen DC. Distributed hierarchical processing in the primate cerebral cortex. *Cereb Cortex*. 1991; 1: 1-47.
2. Purves D, Lotto RB, Williams SM, Nundy S, Yang Z. Why we see things the way we do: evidence for a wholly empirical strategy of vision. *Philos Trans R Soc Lond B Biol Sci*. 2001; 356: 285-297.
3. Nikolic D, Hausler S, Singer W, Maass W. Distributed fading memory for stimulus properties in the primary visual cortex. *PLoS Biol*. 2009; 7: e1000260.
4. Shuler MG, Bear MF. Reward timing in the primary visual cortex. *Science*. 2006; 311: 1606-1609.
5. Chubykin AA, Roach EB, Bear MF, Shuler MG. A cholinergic mechanism for reward timing within primary visual cortex. *Neuron*. 2013; 77: 723-735.
6. Han F, Caporale N, Dan Y. Reverberation of recent visual experience in spontaneous cortical waves. *Neuron*. 2008; 60: 321-327.
7. Liang F, Xiong XR, Zingg B, Ji XY, Zhang LI, et al. Sensory cortical control of a visually induced arrest behavior via corticotectal projections. *Neuron*. 2015; in press.
8. Xu W, Huang X, Takagaki K, Wu JY. Compression and reflection of visually evoked cortical waves. *Neuron*. 2007; 55: 119-129.
9. Benucci A, Frazor RA, Carandini M. Standing waves and traveling waves distinguish two circuits in visual cortex. *Neuron*. 2007; 55: 103-117.
10. Dick AO. Iconic memory and its relation to perceptual processing and other memory mechanisms. *Percep Psychophys*. 1974; 16: 575-596.
11. Averbach E, Sperling G. Short-term storage of information in vision. In: Cherry C,

editor. *Information Theory*. London: Butterworth; 1961.

12. Super H, Spekreijse H, Lamme VA. A neural correlate of working memory in the monkey primary visual cortex. *Science*. 2001; 293: 120-124.
13. Munneke J, Heslenfeld DJ, Theeuwes J. Spatial working memory effects in early visual cortex. *Brain Cogn*. 2010; 72: 368-377.
14. Harrison SA, Tong F. Decoding reveals the contents of visual working memory in early visual areas. *Nature*. 2009; 458: 632-635.
15. Amit DJ. The Hebbian paradigm reintegrated: local reverberations as internal representations. *Behav Brain Sci*. 1995; 18: 617-657.
16. Wang XJ. Synaptic reverberation underlying mnemonic persistent activity. *Trends Neurosci*. 2001; 24: 455-463.
17. Ringach DL, Hawken MJ, Shapley R. Dynamics of orientation tuning in macaque primary visual cortex. *Nature*. 1997; 387: 281-284.
18. Benucci A, Ringach DL, Carandini M. Coding of stimulus sequences by population responses in visual cortex. *Nat Neurosci*. 2009; 12: 1317-1324.
19. Brascamp JW, Knapen TH, Kanai R, van Ee R, van den Berg AV. Flash suppression and flash facilitation in binocular rivalry. *J Vis*. 2007; 7: 12 11-12.
20. Fischer J, Whitney D. Serial dependence in visual perception. *Nat Neurosci*. 2014; 17: 738-743.
21. Maljkovic V, Nakayama K. Priming of pop-out: I. Role of features. *Mem Cognit*. 1994; 22: 657-672.
22. Kahneman D, Treisman A, Gibbs BJ. The reviewing of object files: object-specific integration of information. *Cogn Psychol*. 1992; 24: 175-219.
23. Boynton GM, Finney EM. Orientation-specific adaptation in human visual cortex. *J*

- Neurosci. 2003; 23: 8781-8787.
24. Weigelt S, Muckli L, Kohler A. Functional magnetic resonance adaptation in visual neuroscience. *Rev Neurosci.* 2008; 19: 363-380.
 25. Movshon JA, Lennie P. Pattern-selective adaptation in visual cortical neurones. *Nature.* 1979; 278: 850-852.
 26. Haider B, Krause MR, Duque A, Yu Y, Touryan J, et al. Synaptic and network mechanisms of sparse and reliable visual cortical activity during nonclassical receptive field stimulation. *Neuron.* 2010; 65: 107-121.
 27. Niell CM, Stryker MP. Modulation of visual responses by behavioral state in mouse visual cortex. *Neuron.* 2010; 65: 472-479.
 28. Sakata S, Harris KD. Laminar structure of spontaneous and sensory-evoked population activity in auditory cortex. *Neuron.* 2009; 64: 404-418.
 29. de Kock CP, Bruno RM, Spors H, Sakmann B. Layer- and cell-type-specific suprathreshold stimulus representation in rat primary somatosensory cortex. *J Physiol.* 2007; 581: 139-154.
 30. Crochet S, Poulet JF, Kremer Y, Petersen CC. Synaptic mechanisms underlying sparse coding of active touch. *Neuron.* 2011; 69: 1160-1175.
 31. Kendall MG, Stuart A, Ord JK, Arnold SF, O'Hagan A. Kendall's advanced theory of statistics. New York: Halsted Press; 1994.
 32. Bedard C, Kroger H, Destexhe A. Modeling extracellular field potentials and the frequency-filtering properties of extracellular space. *Biophys J.* 2004; 86: 1829-1842.
 33. Mohajerani MH, Chan AW, Mohsenvand M, LeDue J, Liu R, et al. Spontaneous cortical activity alternates between motifs defined by regional axonal projections.

- Nat Neurosci. 2013; 16: 1426-1435.
34. Herbert H, Jasper MD. Report of the committee on methods of clinical examination in electroencephalography 1957. *Electroencephalography Clin Neurophysiol.* 1957; 10: 370-375.
 35. Sachidhanandam S, Sreenivasan V, Kyriakatos A, Kremer Y, Petersen CC. Membrane potential correlates of sensory perception in mouse barrel cortex. *Nat Neurosci.* 2013; 16: 1671-1677.
 36. Volgushev M, Vidyasagar TR, Pei X. Dynamics of the orientation tuning of postsynaptic potentials in the cat visual cortex. *Vis Neurosci.* 1995; 12: 621-628.
 37. Pei X, Vidyasagar TR, Volgushev M, Creutzfeldt OD. Receptive field analysis and orientation selectivity of postsynaptic potentials of simple cells in cat visual cortex. *J Neurosci.* 1994; 14: 7130-7140.
 38. Hubel DH, Wiesel TN. Receptive fields of single neurones in the cat's striate cortex. *J Physiol.* 1959; 148: 574-591.
 39. Drager UC. Receptive fields of single cells and topography in mouse visual cortex. *J Comp Neurol.* 1975; 160: 269-290.
 40. Metin C, Godement P, Imbert M. The primary visual cortex in the mouse: receptive field properties and functional organization. *Exp Brain Res.* 1988; 69: 594-612.
 41. Niell CM, Stryker MP. Highly selective receptive fields in mouse visual cortex. *J Neurosci.* 2008; 28: 7520-7536.
 42. Liu BH, Li YT, Ma WP, Pan CJ, Zhang LI, et al. Broad inhibition sharpens orientation selectivity by expanding input dynamic range in mouse simple cells. *Neuron.* 2011; 71: 542-554.
 43. Priebe NJ, Ferster D. Inhibition, spike threshold, and stimulus selectivity in primary

- visual cortex. *Neuron*. 2008; 57: 482-497.
44. Ferster D, Miller KD. Neural mechanisms of orientation selectivity in the visual cortex. *Annu Rev Neurosci*. 2000; 23: 441-471.
 45. Benucci A, Saleem AB, Carandini M. Adaptation maintains population homeostasis in primary visual cortex. *Nat Neurosci*. 2013; 16: 724-729.
 46. Dragoi V, Rivadulla C, Sur M. Foci of orientation plasticity in visual cortex. *Nature*. 2001; 411: 80-86.
 47. Prusky GT, Alam NM, Beekman S, Douglas RM. Rapid quantification of adult and developing mouse spatial vision using a virtual optomotor system. *Invest Ophthalmol Vis Sci*. 2004; 45: 4611-4616.
 48. Binzegger T, Douglas RJ, Martin KA. A quantitative map of the circuit of cat primary visual cortex. *J Neurosci*. 2004; 24: 8441-8453.
 49. Lefort S, Tómm C, Floyd Sarria JC, Petersen CC. The excitatory neuronal network of the C2 barrel column in mouse primary somatosensory cortex. *Neuron*. 2009; 61: 301-316.
 50. Jia H, Rochefort NL, Chen X, Konnerth A. Dendritic organization of sensory input to cortical neurons in vivo. *Nature*. 2010; 464: 1307-1312.
 51. Ko H, Hofer SB, Pichler B, Buchanan KA, Sjöström PJ, et al. Functional specificity of local synaptic connections in neocortical networks. *Nature*. 2011; 473: 87-91.
 52. Hofer SB, Ko H, Pichler B, Vogelstein J, Ros H, et al. Differential connectivity and response dynamics of excitatory and inhibitory neurons in visual cortex. *Nat Neurosci*. 2011; 14: 1045-1052.
 53. Li Y, Lu H, Cheng PL, Ge S, Xu H, et al. Clonally related visual cortical neurons show similar stimulus feature selectivity. *Nature*. 2012; 486: 118-121.

54. Yu YC, Bultje RS, Wang X, Shi SH. Specific synapses develop preferentially among sister excitatory neurons in the neocortex. *Nature*. 2009; 458: 501-504.
55. Ohtsuki G, Nishiyama M, Yoshida T, Murakami T, Histed M, et al. Similarity of visual selectivity among clonally related neurons in visual cortex. *Neuron*. 2012; 75: 65-72.
56. Song S, Sjöström PJ, Reigl M, Nelson S, Chklovskii DB. Highly nonrandom features of synaptic connectivity in local cortical circuits. *PLoS Biol*. 2005; 3: e68.
57. Sadovskiy AJ, MacLean JN. Mouse visual neocortex supports multiple stereotyped patterns of microcircuit activity. *J Neurosci*. 2014; 34: 7769-7777.
58. Guillery RW, Sherman SM. Thalamic relay functions and their role in corticocortical communication: generalizations from the visual system. *Neuron*. 2002; 33: 163-175.
59. Manita S, Suzuki T, Homma C, Matsumoto T, Odagawa M, et al. A Top-Down Cortical Circuit for Accurate Sensory Perception. *Neuron*. 2015; 86: 1304-1316.
60. Lavzin M, Rapoport S, Polsky A, Garion L, Schiller J. Nonlinear dendritic processing determines angular tuning of barrel cortex neurons in vivo. *Nature*. 2012; 490: 397-401.
61. Palmer LM, Shai AS, Reeve JE, Anderson HL, Paulsen O, et al. NMDA spikes enhance action potential generation during sensory input. *Nat Neurosci*. 2014; 17: 383-390.
62. Kleindienst T, Winnubst J, Roth-Alpermann C, Bonhoeffer T, Lohmann C. Activity-dependent clustering of functional synaptic inputs on developing hippocampal dendrites. *Neuron*. 2011; 72: 1012-1024.

63. Takahashi N, Kitamura K, Matsuo N, Mayford M, Kano M, et al. Locally synchronized synaptic inputs. *Science*. 2012; 335: 353-356.
64. Druckmann S, Feng L, Lee B, Yook C, Zhao T, et al. Structured synaptic connectivity between hippocampal regions. *Neuron*. 2014; 81: 629-640.
65. Smith SL, Smith IT, Branco T, Hausser M. Dendritic spikes enhance stimulus selectivity in cortical neurons in vivo. *Nature*. 2013; 503: 115-120.
66. Dehaene S, Naccache L, Le Clec HG, Koechlin E, Mueller M, et al. Imaging unconscious semantic priming. *Nature*. 1998; 395: 597-600.
67. Fiser J, Biederman I. Invariance of long-term visual priming to scale, reflection, translation, and hemisphere. *Vision Res*. 2001; 41: 221-234.
68. Lamme VA, Roelfsema PR. The distinct modes of vision offered by feedforward and recurrent processing. *Trends Neurosci*. 2000; 23: 571-579.
69. Liu T, Stevens ST, Carrasco M. Comparing the time course and efficacy of spatial and feature-based attention. *Vision Res*. 2007; 47: 108-113.
70. Watanabe T, Harner AM, Miyauchi S, Sasaki Y, Nielsen M, et al. Task-dependent influences of attention on the activation of human primary visual cortex. *Proc Natl Acad Sci U S A*. 1998; 95: 11489-11492.
71. Vidyasagar TR. Gating of neuronal responses in macaque primary visual cortex by an attentional spotlight. *Neuroreport*. 1998; 9: 1947-1952.
72. Li W, Piech V, Gilbert CD. Perceptual learning and top-down influences in primary visual cortex. *Nat Neurosci*. 2004; 7: 651-657.
73. Poort J, Raudies F, Wannig A, Lamme VA, Neumann H, et al. The role of attention in figure-ground segregation in areas V1 and V4 of the visual cortex. *Neuron*. 2012; 75: 143-156.

74. Jack AI, Shulman GL, Snyder AZ, McAvoy M, Corbetta M. Separate modulations of human V1 associated with spatial attention and task structure. *Neuron*. 2006; 51: 135-147.
75. De Graef P, Verfaillie K. Transsaccadic memory for visual object detail. *Prog Brain Res*. 2002; 140: 181-196.
76. Irwin DE, Andrews R. Integration and accumulation of information across saccadic eye movements. In: Inui T, McClelland JL, editors. *Attention and performance XVI: Information integration in perception and communication*. Cambridge: MIT Press; 1996. pp. 125-155.
77. Irwin DE. Memory for position and identity across eye movements. *J Exp Psychol Learn Mem Cogn*. 1992; 18: 307-317.
78. Minamisawa G, Funayama K, Matsuki N, Ikegaya Y. Intact internal dynamics of the neocortex in acutely paralyzed mice. *J Physiol Sci*. 2011; 61: 343-348.
79. Ishikawa D, Matsumoto N, Sakaguchi T, Matsuki N, Ikegaya Y. Operant conditioning of synaptic and spiking activity patterns in single hippocampal neurons. *J Neurosci*. 2014; 34: 5044-5053.
80. Mohajerani MH, McVea DA, Fingas M, Murphy TH. Mirrored bilateral slow-wave cortical activity within local circuits revealed by fast bihemispheric voltage-sensitive dye imaging in anesthetized and awake mice. *J Neurosci*. 2010; 30: 3745-3751.
81. Shoham D, Glaser DE, Arieli A, Kenet T, Wijnbergen C, et al. Imaging cortical dynamics at high spatial and temporal resolution with novel blue voltage-sensitive dyes. *Neuron*. 1991; 24: 791-802.
82. Brainard DH. The Psychophysics Toolbox. *Spat Vis*. 1997; 10: 433-436.

83. Ban H, Yamamoto H. A non-device-specific approach to display characterization based on linear, nonlinear, and hybrid search algorithms. *J Vis.* 2013; 13: 20.
84. Naruse Y. Development of mobile wireless EEG system with dry electrode. *Proc Life Eng Symp.* 2014; 1: 130-132.
85. Delorme A, Makeig S. EEGLAB: an open source toolbox for analysis of single-trial EEG dynamics including independent component analysis. *J Neurosci Methods.* 2004; 134: 9-21.
86. Swindale NV. Orientation tuning curves: empirical description and estimation of parameters. *Biol Cybern.* 1998; 78: 45-56.
87. Nimmerjahn A, Kirchhoff F, Kerr JN, Helmchen F. Sulforhodamine 101 as a specific marker of astroglia in the neocortex in vivo. *Nat Methods.* 2004; 1: 31-37.
88. Sohya K, Kameyama K, Yanagawa Y, Obata K, Tsumoto T. GABAergic neurons are less selective to stimulus orientation than excitatory neurons in layer II/III of visual cortex, as revealed by in vivo functional Ca²⁺ imaging in transgenic mice. *J Neurosci.* 2007; 27: 2145-2149.
89. Ohki , Chung , Ch'ng Y, Kara , Reid R. Functional imaging with cellular resolution reveals precise micro-architecture i visual cortex. *Nature.* 2005; 43:597-560.
90. Del Cul , Baillet , Dehaene. Brain dynamics underlying the nonlinear threshold for access to consciousness. *PLoS Biol.* 2007 :e26.
91. Funayama , Minamisawa , Matsumoto , Ban , Chan A, Matsuki , Murphy T, Ikegaya. Neocortical Rebound Depolarization Enhances Visual Perception. *PLoS Biol.* 2015; 1:e100223.
92. Takahashi , Sasaki , Matsumoto , Matsuki , Ikegaya. Circuit topology for synchronizing neurons in spontaneously active networks. *Proc Natl Acad Sci U S*

- A. 2010; 10:10244-10244.
93. Yoshimura , Callaway E. Fine-scale specificity of cortical networks depends on inhibitory cell type and connectivity. *Nat Neurosci.* 2005;1552-1552.
 94. Ren , Yoshimura , Takada , Horibe , Komatsu. Specialized inhibitory synaptic actions between nearby neocortical pyramidal neurons. *Science.* 2007; 31:758-756.
 95. Wehr , Zador A. Balanced inhibition underlies tuning and sharpens spike timing in auditory cortex. *Nature.* 2003; 42:442-442.
 96. Higley M, Contreras. Balanced excitation and inhibition determine spike timing during frequency adaptation. *J Neurosci.* 2006; 2:448-445.
 97. Zhang , Xu , Kamigaki , Hoang Do J, Chang W, Jenvay , Miyamichi , Luo , Dan. Selective attention. Long-range and local circuits for top-down modulation of visual cortex processing. *Science.* 2014; 34:660-660.
 98. Lien A, Scanziani. Tuned thalamic excitation is amplified by visual cortical circuits. *Nat Neurosci.* 2013; 1:1315-1312.
 99. Zingg , Hintiryan , Gou , Song M, Bay , Bienkowski M, Foster N, Yamashita , Bowman , Toga A, Dong H. Neural networks of the mouse neocortex. *Cell.* 2014; 15:1096-1011.
 100. Reinhold , Lien A, Scanziani. Distinct recurrent versus afferent dynamics in cortical visual processing. *Nat Neurosci.* 2015; 1:1789-1789.
 101. Halassa M, Siegle J, Ritt J, Ting J, Feng , Moore C. Selective optical drive of thalamic reticular nucleus generates thalamic burst and cortical spindles. *Nat Neurosci.* 2011; 1:1118-1112.
 102. Saalmann Y, Kastner. Gain control in the visual thalamus during perception and cognition. *Curr Opin Neurobiol.* 2009; 1:408-401.

103. Guillery R, Harting J. Structure and connections of the thalamic reticular nucleus: Advancing views over half a century. *J Comp Neurol.* 2003; 46:360-367.
104. Vong , Ye , Yang , Choi , Chua S J, Lowell B. Leptin action on GABAergic neurons prevents obesity and reduces inhibitory tone to POMC neurons. *Neuron.* 2011; 7:142-145.
105. Mease R, Krieger , Groh. Cortical control of adaptation and sensory relay mode in the thalamus. *Proc Natl Acad Sci U S A.* 2014; 11:6798-6780.
106. Van Horn S, Erisir , Sherman S. Relative distribution of synapses in the A-laminae of the lateral geniculate nucleus of the cat. *J Comp Neurol.* 2000; 41:509-502.
107. Peters , Payne B. Numerical relationships between geniculocortical afferents and pyramidal cell modules in cat primary visual cortex. *Cereb Cortex.* 1993; 69-67.

ACKNOWLEDGEMENTS

I am deeply thankful to Prof. Yuji Ikegaya for providing me an education and giving me an opportunity to research for five years of doctoral course. His comments and suggestions were inestimable value for my research, and his creativity often brought breakthroughs to my study whenever it hit a wall. I am also really grateful to him for being a role model as a researcher and teaching me the “how to” on neuroscience research.

My heartfelt appreciation goes to Prof. Norio Matuski whose comments made enormous contribution to my work. He also provided a warm atmosphere in the laboratory, which allowed me to concentrate energetically on my research.

I would also like to express my gratitude to Dr. Ryuta Koyama, Dr. Hiroshi Nomura, and Dr. Takuya Sasaki, Dr. Haruki Takeuchi, Dr. Ai Nakashima for always giving me advices from many different point of views. They taught me the ways to have discussions with scientists of different research background.

I would specially thank Dr. Genki Minamisawa, from whom I learned the skills of in vivo electrophysiology, and learned the basis of sensory processes of neocortices. I also would like to thank him for introducing me to savate.

I am grateful to my colleagues in the PhD course, Chiaki Kobayashi, Daisuke Nakayama, Hiroaki Norimoto, Nobuyoshi Matsumoto, Yuuki Miura. I would not be able to come this far without their beings. They are my comrades in arms.

I would like to thank Sakiko Toyoda, Natsuko Hitora, Reimi Abe for being such great neighbors as well as being great advisors of my life. They always enlighten me and brought me courage to move forward whenever it seems that there is no light. My life at lab became really fun because of them.

I sincerely am grateful for Hiroshi Ban, Allen W Chan, Timothy H Murphy for contributing to my flash paper. With their support, my paper has improved extensively.

I would like to appreciate all other members of the lab, who made me grow not only as a scientist, but also as an adult: Reiko Sasaki, Naho Hosaka, Soichiro Nakahara, Atushi Usami, Mika Mizunuma, Huliaan Shen, Kentaro Tao, Mari Sajo, Koichi Hashikawa, Ayako Honda, Daisuke Ishikawa, Daisuke Miyamoto, Yuji Takahara, Naoko Homma, Emi Shimizu, Hiroshi Shimagami, Fumitaka Masuda, Saori Okada, Hiroko Osamura, Kazuki Shibata, Testuya Sakaguchi, Hikaru Igarashi, Masamitsu Naka, Kosuke Miyajima, Masataka Ishizuka, Emi Tomikawa, Hirokazu Iwata, Zohal Baraki, Tomoe Ishikawa, Koshiro Hara, Kosuke Onoue, Tomoya Kitagawa, Chie Teshirogi, Takeyuki Miyawaki, Yuka Kasahara, Kohhei Morishita, ZShiwen Zhou, Hideki Ueda, Yusuke Watanabe, Kazuki Okamoto, Hiroki Sugiyama, Nariaki Uemura, Satoshi Iwasaki, Kenichi Makino, Mami Okada, Hiroto Kojima, Cog Lao, Xuezhun Sun, Hideyoshi Igata, Ryota Nakayama, Naoki Ihara, Yuki Takagi, Hiroki Sugiyama, Xuezhun Sun, Yuya Nishimura, Yutaka Hosi, Cong Luo, Yuki Aoki, Megumi Andoh, Sakura Okada, Menguxuan Gao, Toshimitsu Hiragi.

Most importantly, I would like to thank my family, Hironobu Funayama, Uiko Funayama, Kota Funayama, Maiko Funayama, Mamiko Funayama, and Ritsuko Funayama, who have always supported me and respected my decisions for all of my life.